![UAB - Universitat Autònoma de Barcelona]

**Facultat de Ciències**

| Bachelor's thesis | Ruthenium Nanoparticles for the (Photo)catalytic Hydrogen-evolving reaction |

Directors: Xavier Sala Román,
Jordi García-Antón Aviñó

Víctor Pérez Padilla

June 2017

*Nothing in life is to be feared, it is only to be understood. Now is the time to understand more, so that we may fear less.*

MARIE CURIE

## Acknowledgements

**Summary**

Hydrogen gas is regarded as the next generation green fuel. Nevertheless, its production presents several drawbacks such as $CO_2$ emission from natural gas steam reforming, its actual main mode of generation. For that reason is critical to achieve an alternative and environmental friendly path for its mass production.

Water splitting is meant to be the answer to the problem. It uses water, an inexhaustible raw material, for the generation of $H_2$ and $O_2$. The energy for the redox reaction can be supplied from manifold sources, although the object of study of the present report is to focus on photocatalytic water splitting since it uses sunlight as the ultimate source of energy.

Photocatalytic water splitting uses a photosensitizer to convert solar energy into chemical energy, meaning that upon irradiation, electron excitation and transferral arise. In the hydrogen evolution reaction (HER), also called proton reduction, the reduction semi-reaction of water splitting, the catalyst captures the electrons withdrawn from the photosensitizer, which are previously provided from the oxidation semi-reaction of water to dioxygen, to reduce protons into dihydrogen.

It is of great interest to develop efficient (low onset overpotential), active (high TOF) and robust (high TON) non-toxic catalysts for both the water oxidation and the proton reduction reactions. The present report focus on the photocatalytic proton reduction semi-reaction by using a concrete set of ruthenium nanoparticles as catalysts and the posterior optimization of the photocatalytic system employed.

The first photocatalytic studied system consists of a photosensitizer, an electron mediator, a catalyst (Ru NPs) and sacrificial electron species. Photocatalytic systems are highly complex. Additionally, one sole research group has been working with systems similar to those treated in the present report. In order to achieve measurable hydrogen responses these systems need a lot of optimization. The incapability of our systems to provide reasonable hydrogen signals was thought to lie in the poor interaction between the systems' components (low electron transfer rates).

An alternative to the first photocatalytic system consists in ruthenium nanoparticles deposited onto graphene oxide quantum dots (GQDs) hybrid materials embedded onto the surface of a major photoactive $N-TiO_2$ matrix forming a cake-like system (Ru@GQDs@N-TiO_2), where the GQDs are acting as a linking-conductive-intermediate enhancing the interaction between components. For that purpose, ruthenium nanoparticles were impregnated and [Ru(cod)(cot)] decomposed onto graphene oxide quantum dots in order to obtain the hybrid material (Ru@GQDs).

**Table of contents**

**Table of figures**

**Table of tables**

**Table of abbreviations**

| | |
|---|---|
| **CNT** | Carbon Nanotubes |
| **CV** | Cyclic Voltammetry |
| **CP** | Chronopotentiometry |
| **EM** | Electron Mediator |
| **GC-RDE** | Glassy Carbon Rotating Disk Electrode |
| **GHG** | Greenhouse Gas |
| **GQDs** | Graphene Quantum Dots |
| **HER** | Hydrogen-Evolving Reaction |
| **ICIQ** | Institut Català d'Investigació Química |
| **IUPAC** | International Union of Pure and Applied Chemistry |
| **MECD** | Ministerio de Educación, Cultura y Deporte |
| **MOF** | Metal-organic Framework |
| **MTOE** | Million Tone of Oil Equivalent |
| **MV$^{2+}$** | Methyl viologen |
| **NPs** | Nanoparticles |
| **OER** | Oxygen-Evolving Reaction |
| **OPV** | Organic Photovoltaics |
| **PMAID** | 9-phenyl-10-methyl-acridinium ion derivatives |
| **PRC** | Proton Reduction Catalyst |
| **PS** | Photosensitizer |
| **SCE** | Saturated Calomel Electrode |
| **SDS** | Safety Data Sheet |
| **SEA** | Sacrificial Electron Acceptor |
| **SED** | Sacrificial Electron Donor |
| **SelOxCat** | Selective Oxidation Catalysis |
| **TOF** | Turnover Frequency |
| **TON** | Turnover Number |
| **TPES** | Total Primary Energy Supply |
| **TW / W** | Terawatt / Watt |
| **WE** | Working Electrode |
| **WOC** | Water Oxidation Catalysis |

## 1. Introduction

Energy is the base of life and modern society. Electricity represents one of society's greatest needs and concerns. Thus, the development and survival of advanced countries critically depends on access to a regular and secure electrical supply. In the last few decades, the accelerated rate of consumption of fossil fuels (see **Figure 1)**, the actual main source of energy, does not respond to the ever increasing global energy expenditure, neither in the long nor medium term [1]. Additionally, the combustion of fossil fuels is regarded as the major anthropogenic factor contributing to climate change [2], [3].
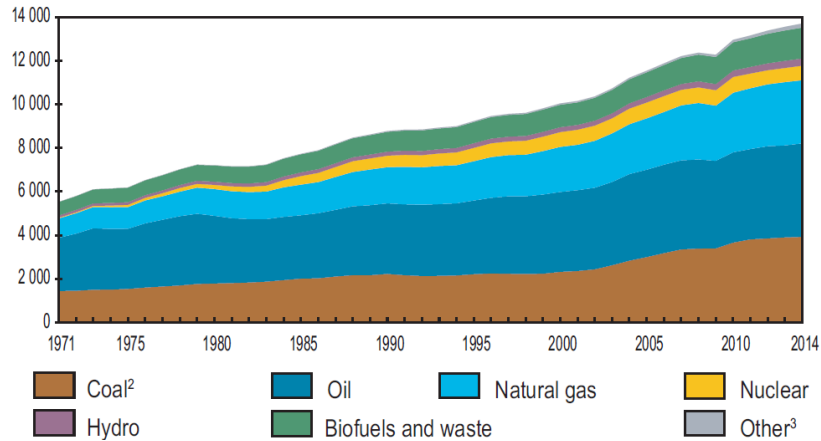


**Figure 1.** World total primary energy supply (TPES) by fuel (MTOE: Million Tonne of Oil Equivalent). MTOE is approximately 42 gigajoules [4].

The fact that the prolongation of the current trend will lead to an energetic collapse is becoming more evident over time. As specified in **Table 1**, coal will be the single fossil fuel after 2042 in the world, being available until at least 2112. Furthermore, carbon-based technology is increasing alarmingly the concentration of greenhouse-gas in the atmosphere.

If pollution is associated with the never-stopping demand for higher energy production, the environmental situation can easily turn fatal. ''Stabilization of greenhouse-gas concentrations in the atmosphere at a level that would prevent dangerous anthropogenic interference with the climate system...'' cited from the United Nations Framework Convention on Climate Change is mandatory to avoid critical levels of pollution [3].

Hence energy sources are a great concern and topic of discussion either in the political, cultural and scientific panorama and they represent a central axis of development for the scientific community worldwide [5].

**Table 1.** Fossil fuels reserves depletion time estimated by Klass and New models in years counting from 2007. New model compared to Klass adds the ratio of consumption to reserves [1].

| Model | Ratio of consumption to reserves | | | Klass model | | | New model | | |
|-------|-----|------|-----|-----|------|-----|-----|------|-----|
|       | Oil | Coal | Gas | Oil | Coal | Gas | Oil | Coal | Gas |
| Year  | 40  | 200  | 70  | 34  | 106  | 36  | 35  | 107  | 37  |

In this context, sustainable development and green chemistry advocate for a human development that meets the needs of present generations without compromising future generations by reducing the energy consumption alongside with the employment of renewable materials and energy sources [6]. For these reasons, research in renewable energies is being promoted either by the public and the private sector, trying to find both a solution and an alternative to the wear and tear of fossil fuels.

Investment in renewable energies represents for entities such as countries and companies an identifier of scientific advancement and environmental awareness, driven by today's social pressure, restrictive legislation and even economic benefits. This investment may lead to self-sustained development and gather an overwhelming favourable public opinion [6].

Biomass, hydropower, wind, geothermal and solar energies are the main renewable sources of our times, being the latter on the rise, as it appears to be the most preferred by the public opinion [7], [8]. Henceforth, this study will focus in detail in solar energy and its applications.

In 2014, total world energy consumption was 12.5TW ($1.25 \cdot 10^{13}$W), equal to 9.425 MTOE or $3.95 \cdot 10^{20}$J [4]. As it can be seen in **Figure 2**, the Earth receives approximately 89 PW ($8.9 \cdot 10^{16}$W) of solar radiation per year [9]. In other words, total world consumption represents 0.014% of the energy Earth is receiving each year from the Sun. For this reason, one should bet heavily on solar energy.
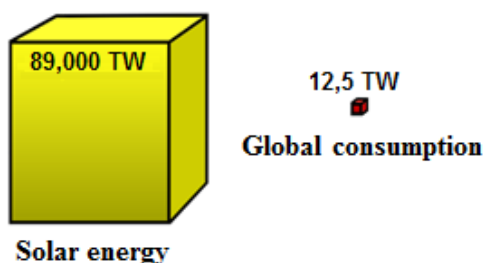


**Figure 2.** The volume of the cubes represents the amount of energy in TW. Yellow-coloured on the left for solar energy and red-coloured on the right for global consumption [10].

Solar energy is a potentially viable substitute for fossil fuels in the future, being one of the cleanest renewable energies with least environmental impact. Diverse strategies have been followed to take advantage of such an enormous amount of energy. The actual problem related to solar technology relays in the inefficiency of the conversion from solar to electrical energy.

Photovoltaic cells are devices designed to produce electrical energy from solar energy by absorbing light with a wavelength between IR and UV. The first photovoltaic cell ever developed was that of Bell Laboratories in the year 1954, with an efficiency of 6%. Thenceforth, it has been achieved a record-breaking efficiency of 25.6% for crystalline silicon devices [11]. On the other hand, non-silicon based devices like organic photovoltaics cells (OPVs) achieve a maximum efficiency of 11.5% [12].

There are still several problems associated with this technology. Some of the materials required for its production are pollutants and its manufacturing processes are very energy-intensive. A cell of crystalline silicon takes approximately 2 years and 3 months to produce the

same energy that has been consumed in its production. Therefore there is a lot of research to be done in this area, leading to more efficient production processes and newer low-cost materials that are not harmful to the environment.

Rather than photovoltaics our interest is to focus in a totally different application of solar energy. Water splitting is a chemical reaction consisting in the decomposition of water into the diatomic gases of the forming elements, these are dihydrogen ($H_2$) and dioxygen ($O_2$). In other words, it uses water as a feedstock resource for the production of hydrogen. One of the main advantages of water splitting over photovoltaics is that the first allows to generate a fuel that can be stored while the latter produces electricity that has to be immediately spent. Water splitting can be performed by electrolysis [13], radiolysis [14], thermolysis [15], photoelectrolysis [16], photobiologically (algae bioreactor) [17] and photocatalitically.

The water splitting reaction (**eq. 1**) is a thermodynamically unfavourable process with a large positive increment of Gibbs free energy ($\Delta G_0$=+237.2 kJ·mol$^{-1}$) [18]. However, the reaction is entropically favourable.

$$H_2O_{(l)} \rightleftharpoons \frac{1}{2} O_{2(g)} + H_{2(g)} \ (1)$$
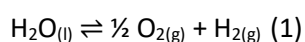
The electrolysis method consists in the decomposition of water into $H_2$ and $O_2$ by directly applying an electrical current through the water which induces redox reactions. Photoelectrolysis is based in the same principle than that of electrolysis with the difference that the electrical energy is supplied by photovoltaics. In comparison, photocatalysis converts directly the solar energy into hydrogen gas by a one-step reaction, therefore it can be a more efficient process than the others [18].

Paracelsus discovered the gas hydrogen in the Middle Age (sixteenth century) by reacting sulfuric acid with iron, called back then ''inflammable air.'' In 1766, Cavendish realized that hydrogen gas combustion resulted in the production of only water. In 1783, Meunier, Laplace and Lavoisier showed that water is formed by one equivalent of oxygen and two equivalents of hydrogen. Lavoisier proposed the name hydrogen to imply that it is a component of water (hydro). In 1784, the first technology to produce dihydrogen at industrial scale was patented by Lavoisier and Meunier, the steam-iron process [14].

Hydrogen is the most abundant chemical element in the universe. It has the lowest molecular weight (MW), the largest thermal conductivity amidst all gases, a large calorific value, the lowest viscosity, the simplest molecular structure and a high reactivity as hydrogen loses easily its valence electron. Problems related to hydrogen are its low density impeding to keep it efficiently in a condensed phase and the consequently lowest hydrogen' heating value per unit of volume compared to other fuels. However, hydrogen has a larger power generation efficiency compared to conventional fuels [14].

The production of hydrogen gas from solar energy by means of water splitting is highly desirable as a route to achieve renewable and clean energy, thus being a major axis for hydrogen economy. Dihydrogen is regarded as the next generation green fuel, since its combustion releases water as the only by-product. Additionally, it can be generated by low or zero-carbon sources as the aforementioned. Hydrogen future is to replace fossil fuels in order

to reduce greenhouse gases (GHG) emission, yet most hydrogen is nowadays produced by steam reforming from natural gas resulting in the latter emission of carbon dioxide [19], [20].

Electrolytic water splitting requires huge amounts of energy which practically makes the process uncompetitive against steam reforming of natural gas or $H_2$-production from coal. In general, the amount of electricity needed is of more value than the $H_2$ produced, resulting in a not widely used process. Nevertheless, hydrogen gas can be used as a complement to store renewable produced electricity when it is not needed, for example at night, and then used during the day when it is most needed.

The photocatalytic method consists in the direct conversion of solar energy into hydrogen solving the energetic intake issue. Water splitting is divided into two semi-reactions: water oxidation, **eq. 2**, also known as oxygen-evolving reaction (OER), yielding oxygen and proton reduction, **eq. 3**, also known as hydrogen evolving reaction (HER), yielding hydrogen. Water oxidation is a thermodynamic and kinetic demanding process since it requires the breakage of two O-H bonds and the extraction of 4 electrons from two water molecules together with the formation of a new O=O double bond. As the water oxidation process is thermodynamically unfavourable it needs to be coupled to an energy input, for example sunlight.

$$2\ H_2O_{(l)} \rightleftharpoons 4\ H^+_{(aq)} + O_{2(g)} + 4\ e^-\ (2)$$

$$4\ H^+_{(aq)} + 4\ e^- \rightleftharpoons 2\ H_{2(g)}\ (3)$$
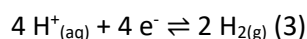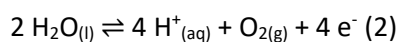
Proton reduction is also a kinetically demanding process. It is thermodynamically more favoured in acidic pH than neutral or basic while water oxidation is less unfavourable in basic pH than neutral or acid.

Water oxidation catalysts (WOC) and proton reduction catalyst (PRC) both increase the reaction rate and minimise the onset overpotential. The overpotential of a catalyst is the increase of potential with respect to the thermodynamic potential of the reaction. The onset overpotential and the overpotential at 10 mA/cm$^2$, for both the lower the better, are the two major benchmarking parameters for proton reduction catalysts. In general, an ideal catalyst (PRC or WOC) is enforced to possess high stability, high efficiency, low toxicity, low overpotential and low cost.

The proposed mechanism for proton reduction on surfaces and in acidic aqueous media is via three elementary reactions known as the Volmer (**eq. 4**) reaction for the proton adsorption and either Tafel (**eq. 5**) or Heyrovsky (**eq. 6**) reactions for the hydrogen gas desorption, where H$^*$ stands for a chemisorbed hydrogen atom:

$$H^+ + e^- \rightarrow H^*\ (4)$$

$$2\ H^* \rightarrow H_2\ (5)$$

$$H^* + H^+ + e^- \rightarrow H_2\ (6)$$
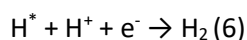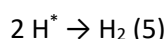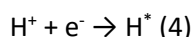
The size of a nanoparticle is an important parameter affecting its proton reduction mechanism. The stabilizing agents tune the size of NPs since the latter is closely related to the electronic and steric effects of the capping ligands, solvents or matrixes. For a concrete amount of matter, smaller NPs will have larger active area than bigger ones. Besides, the size of the Ru

NPs have an effect on the reaction rate for the 'proton reduction' and 'hydrogen-atom association' steps [21] as can be seen in **Figure 3**.
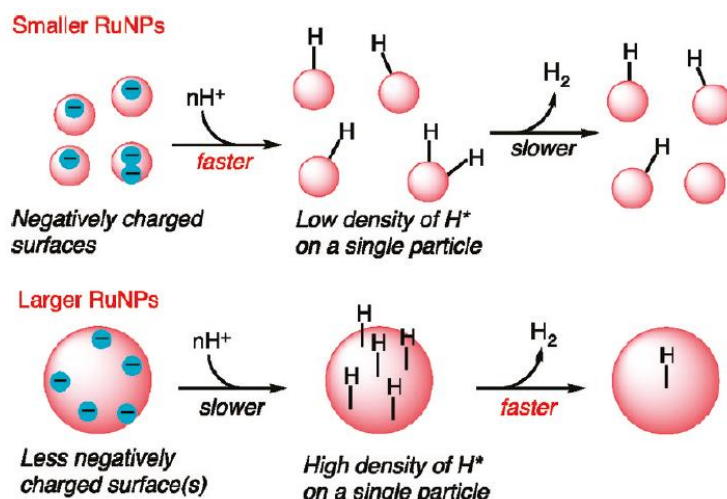


**Figure 3.** Mechanistic scheme for the hydrogen-evolving reaction catalysed by Ru NPs and Ru NPs' size effect on the reaction rate for the 'hydrogen-atom association' and 'proton reduction' steps [21].

On one hand, small NPs present higher negative density easing the hydrogen-atom association step but hindering the proton reduction process. On the other hand, bigger NPs ease the proton reduction process but hinder the hydrogen-atom association step. The best results are then given by particles of intermediate size.

The hydrogen-metal (H-M) bond is also playing a crucial role in proton reduction, high H-M binding energy eases the adsorption of hydrogen but hardens the product desorption. On the other hand, low H-M binding energy results in the opposite effect. Platinum is at the centre of the volcano plot for proton reduction catalysts since it possess the optimum H-M binding energy, which is neither too low nor too high.

Ruthenium presents a slightly weaker H-M ($\sim$65 kcal·mol$^{-1}$) and a stronger HO-M binding values compared to Pt, which slightly decrease the HER efficiency. However, one of the advantages when using Ru is that the binding and dissociation of $H_2O$ (related to H-M and HO-M) on its surface is much more favourable and faster than in Pt offering a much faster proton supply, especially under neutral and basic conditions [22].

Platinum is namely the main hydrogen-evolving catalyst reported due to its low overpotential. However, ruthenium presents similar electrocatalytic activities and properties for proton reduction than that of platinum. Remarkably, a ruthenium-based catalyst (Ru@$C_2$N), similar and for some features superior than the classic Pt/C, has been reported by Jong-Beom Baek et al. [22]. Ruthenium, as platinum, is one of the tenth least abundant elements in the universe (4 ppb), with lesser abundance than that of gold or silver for example. In despite, ruthenium is more abundant than platinum and its cost is only the 4% of the latter [22].

## 1.1. Introduction to the system
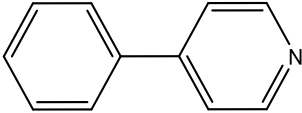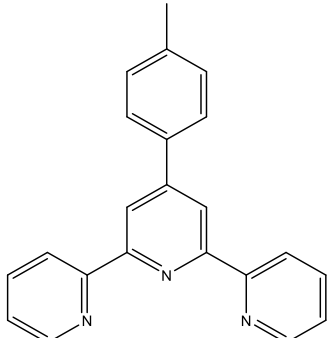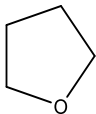
The Ru NPs employed in this work (see **Table 2**) are high surface over volume systems composed of a metallic ruthenium core stabilized by capping organic ligands, being the overall system hydrophobic. It has been proven by PhD members of the group that progressive

surface oxidation takes place when the system is exposed to air leading to NPs with a Ru(0) core coated with ruthenium oxide acting as a passivation layer.

The Ru NPs used were synthesised by the organometallic approach. The method consists in the decomposition of an organometallic precursor [Ru(cod)(cot)] with hydrogen (reducing agent) in the presence of a stabilizing ligand, solvent (THF) or any other system able to stabilize superficially the in situ formed NPs. For instance methylphenylterpyridine, phenylpyridine, phosphine ligands, MeOH/THF or carbon supports (carbon nanotubes (CNT), carbon fibers or carbon dots).

The bonds between ruthenium and its ligands in the complex [Ru(cod)(cot)] (cod = 1,5-cyclooctadiene; cot = 1,3,5-cyclooctatriene) are σ-π. Reducing the double bonds of these ligands results in the release of the metal centre to form Ru NPs. The reduction of these double bonds is carried out under mild conditions: low $H_2$ pressure and room temperature. The [Ru(cod)(cot)] organometallic complex is synthesized from $RuCl_3$ and cyclooctadiene at 90°C in the presence of zinc. The product must be handled with care and kept in inert atmosphere since it easily oxidizes in contact with air [19]. The organometallic approach leads in general to cleaner NPs surfaces compared to solvothermal methods (salt reduction) in which the chlorides from the reduction of $RuCl_3$ can be found on the surfaces.
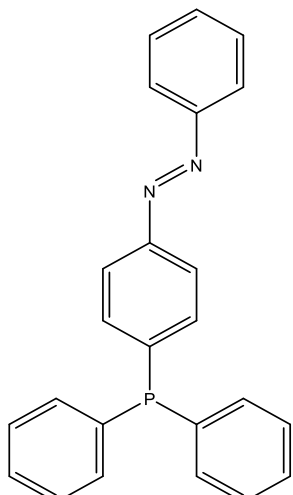
**Table 2.** Ru NPs set used in this work: label, ligand, size and known properties.

| NPs label/code | Stabilizing ligand | Size/diameter (nm)[1] | Electrochemical onset overpotential and overpotential at 10 mA/cm² at pH=0 |
|---|---|---|---|
| Ru-PP | 4-Phenylpyridine (PP)  | 1-2 | Close to 0 mV 20 mV at 10 mA/cm² |
| Ru-MPT | Methylphenylterpyridine (MPT)[2]  | 1-2 | 20 mV 80 mV at 10 mA/cm² |
| Ru-MT | Methanol (MeOH) and tetrahydrofuran (THF)  | 20 | 40 mV 83 mV at 10 mA/cm² |

---

[1] The NPs' diameter (nm) corresponds to an average from their size distribution.

[2] IUPAC name: 4'-(4-Methylphenyl)-2,2':6',2''-terpyridine.

| | Phosphine-based ligand (Ps)[3] | | |
|---|---|---|---|
| Ru-Ps |  | 3 | 115 mV<br>300 mV at 10 mA/cm$^2$ |

The first part of the report consists in the photocatalytic assessment of a system composed of a catalyst (Ru NPs), a sacrificial electron donor (SED), an electron mediator (EM) and a photosensitizer (PS). Due to the results of this part, unexpectedly low, it was appropriate to rethink a new strategy.

The second part of the report is focused on the generation of the hybrid Ru@GQDs material to finally obtain a Ru@GQDs@N-TiO$_2$ photoactive system, where GQDs acts as a linking-conductive-matrix and N-TiO$_2$ as the photoactive species. Graphene quantum dots (GQDs) are highly polar carbon nanoparticles composed mainly of carbon but also, to a lesser extent, oxygen, nitrogen and hydrogen. On their surface they possess several polar groups such as carboxylic acids, alcohols, epoxides, etc. GQDs show many applications in material science and medicine due to their interesting photo-physical properties, specially their luminescence.

GQDs are synthesised by the facile and scalable method of applying a direct discharge of 30 V to two graphitic bars into an aqueous solution at pH 7 and separated 7 cm from one another [23], [24]. The formation of highly reactive oxygen and hydroxyl radicals oxidize the graphitic bar (anode) resulting in the formation of water soluble hydroxylated carbon particles (**eq. 7-10**). These radical species act as 'scissors', cleaving the graphite and consequently producing GQDs with a high content of oxygen in the form of polar groups on their surface.

Oxidative reactions occurring on the anode:

$H_2O \rightarrow 2\ H^+ + 2\ e^- + \frac{1}{2}\ O_2 \uparrow$ (7)

$C_x + H_2O \rightarrow C_xOH + H^+ + e^-$ (8)

$C_x + 2\ H_2O \rightarrow C_{x-1} + CO_2 \uparrow + 4\ H^+ + 4\ e^-$ (9)

$C_x + 4\ H_2O \rightarrow C_{x-2}COOH + CO_2 \uparrow + 7\ H^+ + 7\ e^-$ (10)
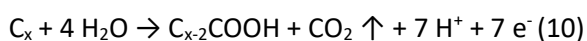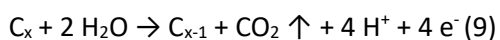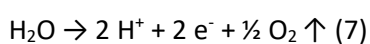
Reductive reaction (**eq. 11**) occurring on the cathode (water reduction):

---

[3] IUPAC name: (E)-1-(4-(diphenylphosphaneyl)phenyl)-2-phenyldiazene.

$$2\ H_2O + 2e^- \rightarrow H_2 \uparrow + 2\ OH^-\ (11)$$
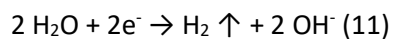
Once synthesised, by means of impregnation (Ru NPs) or decomposition of [Ru(cod)(cot)], the hybrid material Ru@GQDs should be produced. Afterwards, the combined material should be embedded onto the surface of the photoactive $TiO_2$ matrix. Titanum oxide is a ceramic semiconductor material regarded as a promising photocatalyst due to its low cost, high stability and high efficiency. However, practical appliances of $TiO_2$ are limited by its large band gap (3.2 eV) which makes it only respond to UV light (UV light accounts solely about 4% of the solar spectrum while visible light is about 43%) [25]. Then, for practical purposes it is required for $TiO_2$ to absorb in the range of visible light.

The best strategy to achieve visible-light-responsive $TiO_2$ is doping it with non-metal elements (N, C, etc.) or transition metal elements (Pd, Au, Pt, etc.) [26]. Remarkably, $TiO_2$ doped systems have been reported to perform excellently for photocatalytic hydrogen evolution using Ru, Pt, Pd, Au, Rh and Ir as the catalysts [25]. The addition of nitrogen as the doping agent leads to nitrogen doped $TiO_2$ (N-$TiO_2$), narrowing its band gap and being a material capable of harvesting sunlight in the visible light range [27].

**2. Objectives and work distribution**

Objectives:

The scope of this study is to bring some light to the implementation of photocatalytic water splitting and to be one step closer to clean and renewable production of hydrogen gas. A set of functionalized Ru NPs has been widely studied electrochemically as catalysts for proton reduction in non-aqueous solvents by the SelOxCat (Selective Oxidation Catalysis) research but have not yet been neither dispersed in aqueous medium nor photochemically tested. The scope of this study is to cover that gap and perform photocatalytic tests in water. A second general objective is to improve the performance of the photocatalytic system by preparing and characterising new Ru@GQDs hybrid materials to be included in a Ru@GQDs@N-TiO$_2$ system. For this to be done certain guidelines must be followed:

- Acquire a deep knowledge of the state of the art of NPs, water splitting, hydrogen-evolution reaction (HER), metal-organic frameworks (MOFs) and graphene quantum dots (GQDs). Furthermore, finding a relationship between these issues.
- Obtain good dispersions in water of the set of available NPs by means of direct mixture and ultra-sonication or by using MOFs as dispersive matrixes. If MOFs are required, an impregnation methodology is suggested for the introduction of NPs into the MOFs.
- Carry out photocatalytic studies of the systems previously successfully dispersed in water and their subsequent characterization (cyclic voltammetry (CV) and NMR for the photosensitizer [Ru(bpy)]$_3^{2+}$ and hydrogen production for photocatalytic systems).
- Improvement of the photocatalytic system by generating Ru@GQDs hybrids by means of (a) the impregnation of Ru NPs onto GQDs or reduced carbon micro-agglomerates, or (b) the decomposition of [Ru(cod)(cot)] in the presence of GQDs or reduced carbon micro-agglomerates. Characterization of both systems by TEM, SEM, EDX, chronopotentiometry (CP), linear sweep voltammetry (LSV) and photocatalysis.

Work distribution and chronogram:

- Literature reading (3 weeks: 09/01/2017-27/01/2017).
- System preparation and photocatalytic evaluation (8 weeks: 30/01/2017-17/03/2017):
    o Dispersibility tests of Ru NPs in aqueous medium at different pH (1 week: 30/01/2017-03/02/2017).
    o Photosensitizer [(Ru(bpy)$_3$](ClO$_4$)$_2$ synthesis and characterization (1 week: 06/02/2017-10/02/2017).
    o Photocatalytic tests for hydrogen-evolving reaction (6 weeks: 13/02/2017-17/03/2017).
- System improvement (9 weeks: 20/03/2017-24/05/2017, Easter Week not included).
    o GQDs synthesis (1 week: 20/03/2017-24/03/2017).
    o GQDs reduction (1 week: 27/03/2017-31/03/2017).
    o Reduced micro-agglomerate impregnation and [Ru(cod)(cot)] decomposition (5 weeks: 03/04/2017-12/05/2017).
    o GQDs systems' characterization (2 weeks: 15/05/2017-26/05/2017).

## 3. Experimental section

### 3.1. Dispersibility trials of Ru NPs

The dispersibility tests were performed by using 1 mg of each NP, weighted on the microbalance Mettler Toledo MX5 or the analytical balance Mettler Toledo XPE205, added into 2 mL of the respective buffer solution and sonicated for 30 minutes. Qualitative comparisons are established all throughout the report. For these to be objective it has been intended to keep the parameters of the experiences constant, trying to always achieve a high level of reproducibility.

Phosphate buffers were prepared at pH 7 and 12 adjusting the ionic strength at 100 mM with NaCl. An example for that of pH 12 (real pH 11.7) is done by adding 0.0014 mol (0.50g) of $Na_2HPO_4·12H_2O$ (MW=358.12g/mol), 0.0025 mol (0.95g) of $Na_3PO_4·12H_2O$ (380.12g/mol) and 0.024g of NaCl into 200 mL of MilliQ water. The data used to prepare the buffers was collected from reference [28]. pH 0 was achieved by using 1M $H_2SO_4$ aqueous solution.

### 3.2. Synthesis of the photosensitizer [Ru(bpy)₃][ClO₄]₂
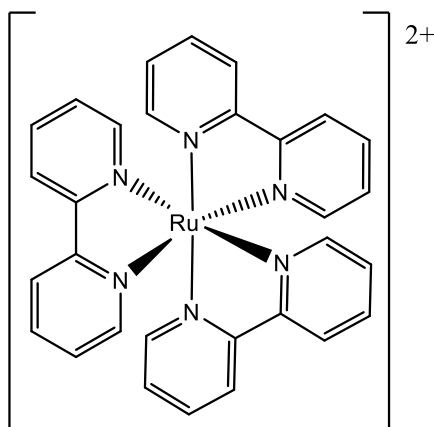


**Figure 4.** [Ru(bpy)₃]²⁺ cation.

350 mg of $RuCl_3·3H_2O$ and 1.000 g of 2,2'-bipyridine (1.6 equivalents, **eq. 12** and **Table 3**) are added to a bottom round flask with 20 mL of EtOH. Then, the bottom round flask is put in a silicone bath with a reflux assembly at 85°C during 36h. After letting the solution cooling down, the unreacted solid (both ruthenium and ruthenium chloride, black coloured solids) is filtered off and discarded. Afterwards the solvent is evaporated in a rotavap (Heidolph Laborota 4001 efficient) under reduced pressure and a reddish precipitate is formed.

Then, 30 mL of $H_2O$ and 5 mL of EtOH are added to the precipitated and 3 extractions with 35 mL of toluene are carried out. These extractions are for the separation of the dissolved and unreacted 2,2'-bipirydine (yellow solution).

$$RuCl_3·3H_2O + \textbf{3} \ 2,2'\text{-bipyridine} + ½ \ EtOH + \textbf{2} \ NaClO_4 \rightarrow$$

$$[Ru(bpy)_3][ClO_4]_2 + \textbf{2} \ NaCl + \textbf{3} \ H_2O + HCl + ½ \ CH_3CHO \ (12)$$
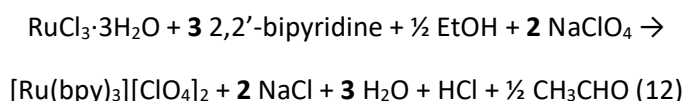
Finally, 600 mg of $NaClO_4$ (1.9 equivalents) are added to the water/ethanol extracted portion in order to displace chloride anions. $NaClO_4$ has to be manipulated in an anhydrous environment ($NaClO_4$ is hygroscopic). The final precipitated, [Ru(bpy)₃][ClO₄]₂ (orange), see the cation chemical structure on                **Figure 4**, is filtered off and dried under vaccum. The obtained orange powder is characterized by ¹H NMR in $D_2O$ (250MHZ/52 MM SPECTROSPIN and BRUKER instrument). This synthetic route was extracted from reference [29] and subsequently modified by an internal protocol provided by the Institut Català d'Investigació Química (ICIQ) with a yield of 70%.

**Table 3.** Relation of reagents for the synthesis of the photosensitizer [Ru(bpy)₃][ClO₄]₂. Equivalents are calculated by Mol. Rel. / Stoich. Rel.

| Reagent | Amount (g) | MW (g·mol$^{-1}$) | mmol | Molecular relation | Stoichiometric relation | Equivalents |
|---|---|---|---|---|---|---|
| RuCl$_3$·3H$_2$O | 0.3525 | 261.42 | 1.348 | 1 | 1 | 1 |
| 2,2'-bipyridine | 1.01 | 156.19 | 6.466 | 4.80 | 3 | 1.6 |
| NaClO$_4$ | 0.613 | 122.44 | 5.007 | 3.714 | 2 | 1.9 |
| [Ru(bpy)$_3$][ClO$_4$]$_2$ | - | 612.35 | - | - | - | - |

The obtained $^1$H NMR spectrum, see **Figure 5**, presents 4 signals corresponding to the expected product, 1 corresponding to the solvent and does not present any impurity peak. Five signals were obtained corresponding to: 4.7 ppm (s, H$_2$O), 7.3 (t, 1H), 7.7 (d, 1H), 8.0 (t, 1H) and 8.4 (d, 1H) as expected for the high symmetry of the ligands and the complex.
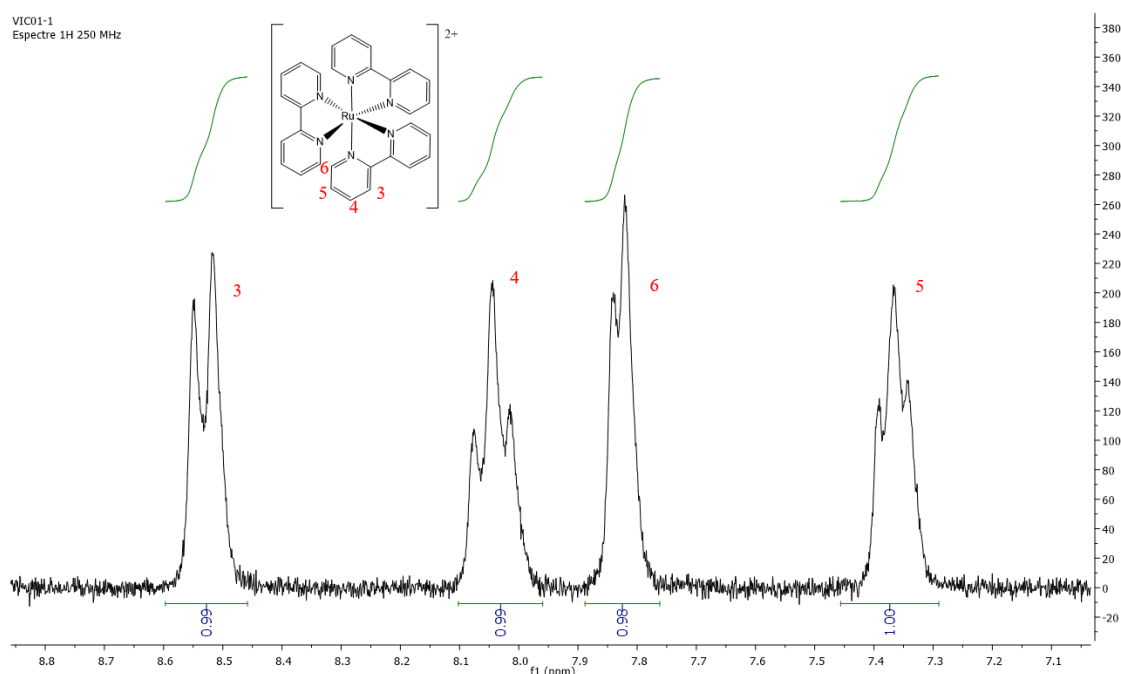


**Figure 5.** $^1$H-NMR (250 MHz, D$_2$O) spectrum for the photosensitizer [Ru(bpy)$_3$][ClO$_4$]$_2$.

Further characterization beyond $^1$H NMR is carried out to ensure the product's nature. The chosen technique is cyclic voltammetry (CV), that allows a facile comparison of the product CV to that registered in the literature for [Ru(bpy)$_3$][ClO$_4$]$_2$ [30]. The potentials (reductive and oxidative waves) of both CVs were identical, meaning that the product corresponds to [Ru(bpy)$_3$][ClO$_4$]$_2$. The CV was performed under the same conditions than that of the literature on a SP-150 BioLogic Science Instruments potentiostat: saturated calomel electrode (SCE) as the reference electrode, Pt as the auxiliary electrode, glassy carbon as the working electrode and Na$_2$SO$_4$ 0.05M aqueous solution. Reduction and oxidation curves for ruthenium cation are registered at 1.05V and 1.1V vs SCE respectively for both spectrum, see **Figure 22** and **Figure 23** in the **Supporting information**.

### 3.3. Photocatalytic experiments

The hydrogen-evolving reaction rate is assessed by using a setup consisting of a borosilicate glass cell with a cooling jacket closed placed at a concrete distance from the light source (ABET TECHNOLOGIES Solar Simulator U.S. Patent 8116017) so that the light impacting the cell is

exactly that of 1 sun. The position is calibrated with a photodiode. The cell is then closed with a septum and hydrogen concentration measurements are made with a hydrogen Clark electrode (UNISENSE H2-NP-9463). Both the Clark electrode and the light source can only be used after a stabilization time period to achieve highly sensitive concentration signals of the evaluated species. In advantage, Clark electrode gives in-time measurements compared to gas chromatography (GC) used by Fukuzumi's group.

Clark electrode and light source are turned on and left to stabilize for 1 hour. The components of the photocatalytic system are consecutively added to a cell covered with foil together with a stirring bar. Oxalate and ascorbic acid are directly added in their solid form. Triethanolamine (TEOA), liquid at room temperature, is also directly added using a micropipette. Ru NPs are added from dispersed stock aqueous solutions after 30 min previous sonication. Methyl viologen ($MV^{2+}$) is also added from a stock aqueous solution. Water is added with a micropipette leaving only a small volume for the posterior addition of the photosensitizer. Then the cell is covered with a septum, the stirring is turned on and the Clark electrode is pricked trough the septum and left 30 min for signal stabilization. The cell is then degassed for 30 min by using an inlet syringe connected to a balloon full of nitrogen and an outlet syringe both pricked though the septum. At that point, the photosensitizer is added from a stock solution by using a syringe bringing to volume the cell. After the addition is fully completed, the purging syringes and balloon and the foil are removed and measurements are taken with the Clark electrode. The addition is made this way to avoid the species reaction before Clark can detect any hydrogen generation. Stock solutions and water addition are buffered when using $NaH_2PO_4/H_3PO_4$.

Calibration of the Clark electrode response is performed by adding known volumes of hydrogen (50, 100, 200 and 500 μL) with a Hamilton syringe to the cell-Clark system from a Schlenk with a balloon containing hydrogen at 1 atm. Following the ideal gas law for a fixed pressure, volume and temperature, amount can be given by $n = (P \cdot V)/(R \cdot T)$. Thus, the relation between voltage and amount (μmol) is obtained from the plot (see **Figure 6**).
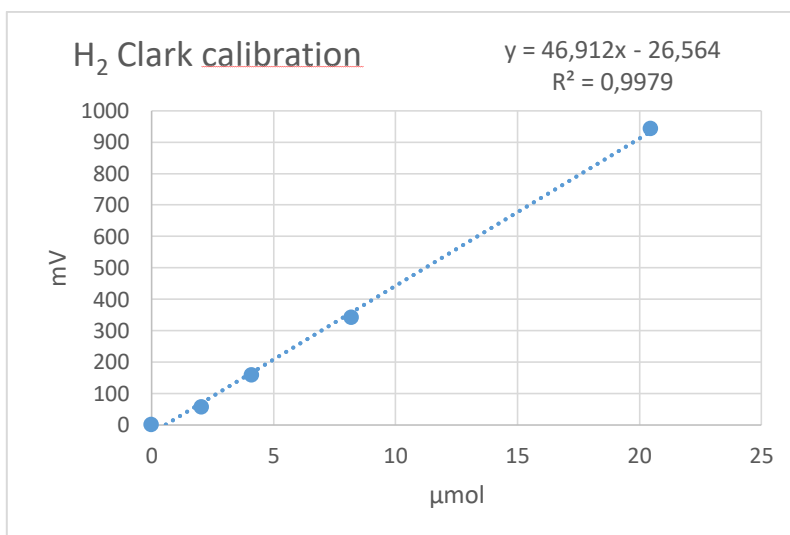


**Figure 6.** Clark response calibration (mV vs μmol) made by the addition of known volumes of $H_2$.

### 3.4. Synthesis of Graphene oxide quantum dots (GQDs)

GQDs are synthesised by the facile and scalable method of applying a direct discharge of 30V (BLAUSONIC EP-613A power supply) to two graphitic bars into an aqueous solution at pH 7 and separated 7 cm from one another [23], [24]. Bubbles are observed on both electrodes: $CO_2$, $O_2$ on the anode (+) and $H_2$ on the cathode (-).

The resultant black solution was filtered twice under vacuum (Kitasato + Büchner) to get rid of bigger particles and the water was evaporated in the rotavap. Finally, the wet solid particles were dried under vacuum line to obtain the final product. TEM (JEOL JEM-1400) and HRTEM (JEOL JEM-2011) were performed to characterize shape and size (see **Figure 7**). The synthesised GQDs' size is comprised between 5-8 nm.
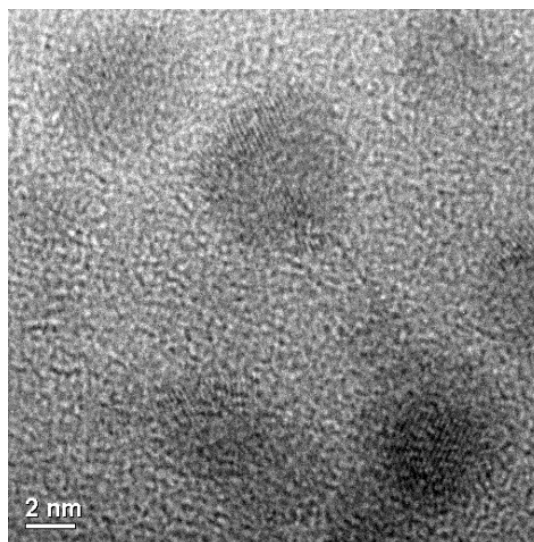


**Figure 7.** HRTEM image of GQDs. Carbon layers within the dot can be distinguished.

### 3.5. Reduction of graphene quantum dots to form carbon micro-agglomerates

20 mg of GQDs are added to 40 mL MilliQ water in a round bottom flask (black-coloured solution). Then 0.2350g of $CaCl_2$ (catalyst) and 0.4550g of $NaBH_4$ (reducing agent) are added and the solution is left stirring for 12 hours (overnight) at room temperature. $CaCl_2$ reacts with $NaBH_4$ to form NaCl and $Ca(BH_4)_2$, the latter reducing more effectively α,β-epoxyketones, α,β-unsaturated ketones and graphene oxide [31]–[34]. The resultant solution is then washed and centrifuged (Centrifuge Cencom II) four times at 3500 rpm for 10 min with hot water (80°C). The wet solid is dried under reduced pressure (vacuum line) to finally obtain a low-density (less dense than parent GQDs) grey-coloured powder. TEM of the reduced material is carried out to characterize shape and size. The compounds, amounts and conditions used were extracted from a paper on graphene oxide reduction [34].

### 3.6. Impregnation of Ru NPs onto graphene oxide quantum dots and reduced micro-agglomerates

0.5 mL of THF containing either 5 mg of GQDs or 5 mg of reduced micro-agglomerate is added to a glass vial together with a previously sonicated solution (30 min) of 0.5 mL of THF containing 0.25 mg of Ru-MPT (5% in weight of Ru NPs to carbon material). The final solution is left in the closed vials stirring 12 hours overnight. Then, THF is dried under vacuum, the material dispersed in water and centrifuged at 3500 rpm for 10 min. After centrifugation, Ru@GQDs presents a supernatant and a precipitate while all the material is precipitated for Ru@reduced micro-agglomerate. TEM of Ru@GQDs precipitate and supernatant and Ru@reduced micro-agglomerate precipitate is then carried out to characterize the properties of the resulting impregnated hybrid materials.

GQDs and reduced micro-agglomerates are also placed in 1 mL THF at room temperature for 12h overnight to monitor their potential self-aggregation under impregnation conditions. TEM images are also obtained for both samples.

### 3.7. Decomposition of [Ru(cod)(cot)] onto graphene oxide quantum dots and reduced micro-agglomerates

Fischer-Porter glass vial is placed in the oven at 80°C for 1 hour to remove residual water from the walls. [Ru(cod)(cot)] is highly sensitive to moisture and oxygen. Following, the Fischer-Porter is removed from the oven and 20 mg of either GQDs or reduced micro-agglomerates are added together with a stirring bar. Then, the Fischer-Porter is closed. Applying a positive nitrogen flux and changing the metallic cap for a septum 4 mL of degassed and dehydrated THF are added with a syringe. The septum is removed and the Fischer-Porter closed, vacuum is applied to the interior. The Fischer-Porter is then placed in a glove-box (MBRAUN systems UNILAB MB-20-G with TP170b) where 3.1 mg of [Ru(cod)(cot)] are added (5% of ruthenium in respect to carbon material). The Fischer-Porter is removed from the glove-box and 3 bar of $H_2$ are added to the interior. The Fischer-Porter is left 4 hours stirring. Finally, the dispersion is placed in a vial, TEM is carried out and THF is evaporated under reduced pressure in the vacuum line.

## 4. Results and discussion

### 4.1. Photocatalytic hydrogen-evolving reaction: general considerations

This first section deals in depth with the theory behind the photocatalytic systems used in the present report. Due to the complexity of these systems it has been found necessary to answer several questions among those one can find: how do they operate? What are the required components? And, what concentrations should be used? This theoretical part then seeks to ease the understanding of the posterior results and discussion and therefore the procedure followed throughout the entire report. It is the first section since chronologically it was also the first performed task: a comprehensive literature research to set the basis of the report.

In water splitting, the oxygen-evolving reaction supplies electrons for proton reduction. However, when assessing the photocatalytic reactions separately there is the need to add species capable of giving/accepting the required electrons, known as sacrificial electron donors/acceptors (SED/SEA) for proton reduction and water oxidation, respectively. These sacrificial electron species are consumed throughout the reaction, thus being the limiting reagents in experimental setups where the rest of components, mainly catalyst and photosensitizer –see below- are stable.

Photocatalytic hydrogen-evolving reactions need several components among which one can find a catalyst, an electron mediator (EM), a photosensitizer (PS) and a sacrificial electron species. The employed catalysts (in this work Ru NPs) ease the reaction by anchoring protons on its surface. The electron mediator transfers the electrons from the photosensitizer to the catalyst, see **Figure 24** in the **Supporting Information** for the chemical structure of these species. The photosensitizer excites upon light irradiation of a certain wavelength and gives an electron to the catalyst, either by direct transfer (donor-acceptor-linked type PS) or through an electron mediator (acceptor type PS). The tested PSs in the present report are $[Ru(bpy)_3]^{2+}$ and ZnTCPP both acceptor PS, for their chemical structure see **Figure 25** in the **Supporting Information**. Finally, the sacrificial electron donor is the ultimate source of electrons being a reductant species. A general overview is shown in **Figure 8**.
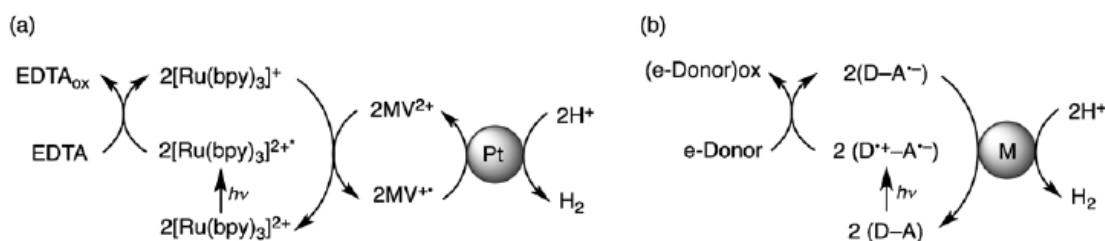


**Figure 8.** (a) Catalytic conventional cycle composed of EDTA (SED), $[Ru(bpy)_3]^{2+}$ (PS), $MV^{2+}$ (EM) and Pt NPs (catalyst). (b) Overall catalytic cycle for a system with a donor-acceptor linked dyad and without an EM [35].

These systems have been constantly under improvement, for instance substituting the electron mediator with a donor-acceptor-linked type photosensitizer, which is able to give the electrons directly to the catalyst without the need of any electron mediator, improving consequently the efficiency of the process. Although synthesis of donor-acceptor-linked type photosensitizers are reported, the synthetic routes involve several complex steps which are far beyond the scope of this study and would precise an own chronogram. These photosensitizers try to mimic natural systems, thus being highly complex molecules [21].

Best reported proton reduction catalysts are those based on Pt nanoparticles (Pt NPs), since Pt has a low over-potential for the conversion of protons into hydrogen. Nevertheless, Pt catalysts are of limited supply and high cost. Thus, research on abundant and inexpensive metals for proton reduction catalysis is of considerable interest. Several metals and metal oxides have been tested and among them Fe, Ni, Co, Cu, Pt and Ru NPs can be found [36][37]. However, catalysts based on nonprecious-metals perform poorly than Pt and Ru-based catalysts, displaying higher onset overpotentials and lower stabilities, since they are susceptible to acid corrosion [22].

Photocatalytic water splitting is based on highly complex systems and the use of ruthenium catalysts for this reaction is relatively recent. Thus, scarce literature was found when searching for similar systems to ours. To date, June 2017, one sole research group has been testing Ru NPs for the photocatalytic hydrogen-evolving reaction (Fukuzumi et al. research group from Osaka University, Japan). Although similar systems, the system $[Ru(bpy)_3]^{2+}$/methyl viologen $(MV^{2+})$/Ru NPs/SED[4] has been never reported to the best of our knowledge. Ruthenium is always found on the literature together with a more efficient electron transfer electron mediator than methyl viologen when using an acceptor photosensitizer or directly with an acceptor-donor photosensitizer [21], [35], [37]–[41].

The components of our system are similar to those of Pt NPs ($[Ru(bpy)_3]^{2+}$/MV/Pt NPs/SED), but Pt has shown to possess higher photocatalytic activity than that of Ru (both present similar electrocatalytic activity) due to the more efficient interaction of platinum with the components of the photocatalytic system. Systems using Ru NPs need further implementation and enhancement to palliate the worse interaction between components and thus worse electron transfer. Important features for the diverse components are described and examined throughout the following lines.

The most important catalyst-related parameter to optimize is its concentration, being 12.5 mg/L the optimum since higher concentrations result in the quenching of the light absorption from the photosensitizer by the black-coloured Ru NPs. Concentrations below 12.5 mg/L result in less activity as activity is proportional to the catalyst concentration until the optimum max point, for these statements see **Figure 9**. The 12.5 mg/L concentration was used repeatedly in our experiments but it was modified in some cases to notice if there was any appreciable change in the overall photocatalytic activity.
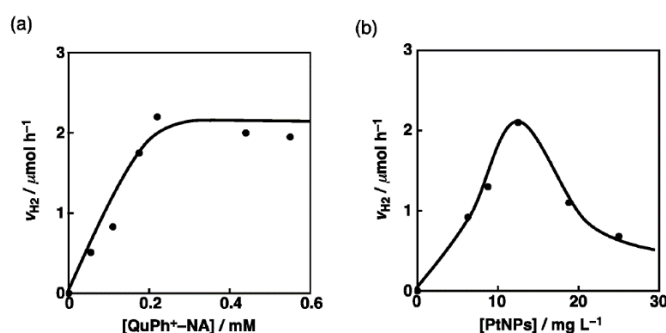


**Figure 9.** On the left (a) Hydrogen-evolution rate vs. PS concentration. On the right (b) Hydrogen-evolution rate vs. catalyst concentration (volcano-type dependence) [39].

[4]Photosensitizer (PS) / Electron Mediator (EM) / Catalyst / Sacrifical Electron Donor (SED)

An ideal electron mediator should efficiently and oxidatively quench the photoexcited photosensitizer and possess slow back electron transfer to the photosensitizer, thus ensuring charge separation. Methyl viologen ($MV^{2+}$) has been extensively studied and reported as an electron mediator for photocatalytic proton reduction due to its low cost and accessibility, although it is unstable during this process. The improvement of its stability is problematic and it lacks of an answer to date. The need to use an electron mediator for our purposes was initially not clear. The experiments were thus performed with and without its presence. An improved due to its strong reducing ability but hard to synthesize electron mediator is that of 9-phenyl-10-methyl-acridinium ion derivatives (PMAID) [38]. For $MV^{2+}$ and/or PMAID chemical structure see **Figure 24** in the **Supporting Information.**

The sacrificial electron donors used are ascorbic / sodium ascorbate pair, triethanolamine (TEOA) and potassium oxalate. Other reported SEDs are NADH (a natural SED but not stable under acidic pH), EDTA, trimethylamine and ethylenediaminetetraacetic acid disodium salt (the last two are synthesised by petroleum-based compounds) [39]. The aforementioned SEDs operate by a 2-electron mechanism, meaning that per each molecule of SED two molecules of PS are reduced. These mechanisms can be found in references [21], [35], [37]–[44]. Upon electronic oxidation the sacrificial electron donors must be irreversible converted into inert molecules to avoid reactions with the negatively charged catalyst where proton reduction is taking place [42].

### 4.2. Dispersibility trials of Ruthenium nanoparticles

Dispersion of Ru NPs in water is of great interest since the hydrogen-evolving reaction is carried out in the present report in aqueous media. The catalyst (Ru NPs) and the photosensitizer ($[Ru(bpy)_3]^{2+}$) must be both in aqueous solution. Water-dispersible NPs are in addition highly desirable in order to avoid the use of organic co-solvents as agents to improve dispersability. An initial strategy before undertaking any dispersability test was to impregnate MOFs (particularly PCN-222, which is available in the research group and forms good dispersions in water) with the Ru NPs [45]–[54]. Therefore, the MOF would act as water-dispersible matrix for the NPs. However, given that we found suitable conditions to disperse the NPs in buffered-water (see **Figure 10** and **Table 4**) no MOF-impregnation tests were finally carried out.

In principle, Ru NPs should be non-soluble and non-dispersible in aqueous solution since they are coated with neutral hydrophobic ligands and the metallic surface possesses no net charge. Solubilisation of the NPs in aqueous solution is not desirable since it would imply the loss of the capping ligands and the oxidation of the metal NPs to the corresponding metal cations. Instead, the goal is to obtain good dispersions in water of the NPs. The Ru NPs were successfully dispersed at a specific pH for each one as shown in **Table 4**.

**Table 4.** Results of the dispersibility trials of Ru NPs.

| NPs label/code | pH | Dispersible? Y/N |
|---|---|---|
| Ru-PP | 0[a] | No |
| | **7[b]** | **Yes** |
| | 11.7[c] | No |
| Ru-PT | **0[a]** | **Yes** |

| | | |
|---|---|---|
| | 7[b] | No |
| | **11.7[c]** | **Yes** |
| Ru-Ps | 0[a] | No |
| | 7[b] | No |
| | **11.7[c]** | **Yes** |
| Ru-MT | **7 (no buffer)** | **Yes** |

[a]$H_2SO_4$, [b]$NaH_2PO_4$ and $H_3PO_4$, [c]$Na_2HPO_4$ and $Na_3PO_4$.

The structure of each NPs' ligand (PP, PT, Ps and MT) can be seen in **Table 2** together with the size of the NPs in nm and their electrochemical parameters. Ru-PP is dispersible in the phosphate buffer solution at pH=7 but it is not when added to pure water. Somehow the buffer is playing an important role in the dispersion of these NPs.

Ru-MT was only tried and successfully dispersed at pH=7 when no buffer was added. This could be explained by the more hydrophilic properties of its ligands, THF and MeOH, solvents that are miscible with water and possess more polar character. Hence, ligands play a crucial role in the operation of these catalysts as they affect their properties (e.g. dispersibility is dependent on the ligands).
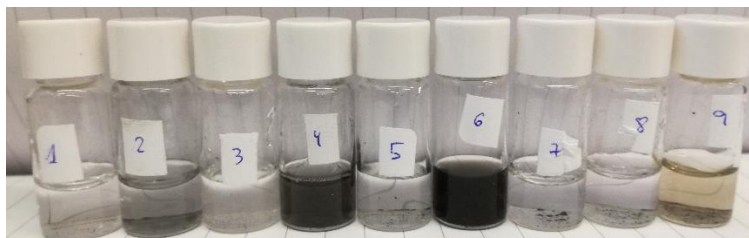


**Figure 10.** Dispersibility trials after sonication. Strong coloured-solution means less agglomerated and more dispersed material.

Dispersibility could be further improved by using mixed solutions of water and acetonitrile (ACN) and, in general, by mixing water with organic water-miscible solvents.

### 4.3. Photocatalytic experiments

The concentrations used in the present report were extracted from Fukuzumi literature and modified subsequently to see if appreciable changes were observable, see **Table 5** for a detailed list of the performed experiments with the particular experimental parameters employed.

**Table 5.** Parameters of the photocatalytic experiments performed in this work.

| Entry | Cell volume (mL) | Catalyst | Photosensitizer | Sacrificial electron species | Electron mediator | pH | Buffer |
|---|---|---|---|---|---|---|---|
| 1 | 3 | Ru-Ps 1 mg | $[Ru(bpy)_3][ClO_4]_2$ $10^{-4}$ M | Ascorbic acid/ascorbate 0.55 M | None | 4.20 | Ascorbic acid/ ascorbate |

| 2 | 3 | Ru-Ps 2 mg | $[Ru(bpy)_3][ClO_4]_2$ $10^{-4}$ M | Ascorbic acid/ascorbate 0.55 M | None | 4.20 | Ascorbic acid/ ascorbate |
|---|---|---|---|---|---|---|---|
| 3 | 3 | Ru-MT 12.5 mg/L | $[Ru(bpy)_3][ClO_4]_2$ $10^{-4}$ M | Ascorbic acid/ascorbate 0.55 M | None | 4.20 | Ascorbic acid/ ascorbate |
| 4 | 4 | Ru-MT 125 mg/L | $[Ru(bpy)_3][ClO_4]_2$ $10^{-4}$ M | Ascorbic acid/ascorbate 0.55 M | None | 4.20 | Ascorbic acid/ascorbate |
| 5 | 4 | Ru-MT 125 mg/L | $[Ru(bpy)_3][ClO_4]_2$ $10^{-4}$ M | TEOA 0.2 M | None | 8.07 | None |
| 6 | 4 | Ru-MT 12.5 mg/L | ZnTCPP $10^{-4}$ M | Ascorbic acid/ascorbate 0.55 M | $MV^{2+}$ 0.3 mM | 4.20 | Ascorbic acid/ascorbate |
| 7 | 4 | Ru-MPT 12.5 mg/L | $[Ru(bpy)_3][ClO_4]_2$ $10^{-4}$ M | Ascorbic acid/ascorbate 0.55 M | None | 4.20 | Ascorbic acid/ ascorbate |
| 8 | 4 | Ru-PP 75 mg/L | $[Ru(bpy)_3][ClO_4]_2$ 0.22 mM | Potassium oxalate 3 mM | None | 7.0 | $NaH_2PO_4/H_3PO_4$ |
| 9 | 4 | Ru-PP 100 mg/L | $[Ru(bpy)_3][ClO_4]_2$ 0.22 mM | Potassium oxalate 3 mM | None | 7.0 | $NaH_2PO_4/H_3PO_4$ |
| 10 | 4 | Ru-PP 12.5 mg/L | $[Ru(bpy)_3][ClO_4]_2$ 0.22 mM | Potassium oxalate 3 mM | $MV^{2+}$ 0.3 mM | 7.0 | $NaH_2PO_4/H_3PO_4$ |

A representative photocatalytic plot is shown in **Figure 11**. The maximum variation of voltage obtained was given by the system described in **Table 5** row **Entry 10** and it was of almost 1 mV (0.02 µmol of $H_2$). In general, systems lacking the electron mediator gave no signal (flat line) while systems including it resulted on hydrogen production. System described in row **Entry 6** produced about 0.69 mV (0.014 µmol of $H_2$).
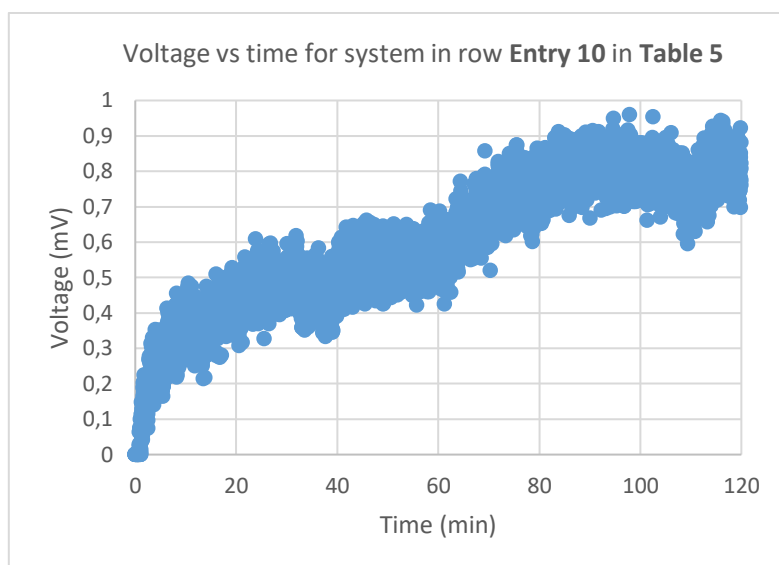
**Figure 11.** Plot of voltage vs time plot for system in row **Entry 10** in **Table 5**.

The plot of voltage vs time was transformed into the variation of evolved $H_2$ vs time by a calibration with known amounts of hydrogen. The maximum production obtained was that of 0.02 µmol by the system described in **Table 5** row **Entry 10** (see **Figure 12**). Although much lower than expected, photocatalytic hydrogen production was successfully achieved. However, there is still a lot of room for the improvement of these systems. Several parameters can be optimised as is the case of pH (buffer species may affect the overall performance), cell volume, dispersibility (mixed solvent method with ACN), amount relations, concentrations and PS, SED, EM and catalyst species.
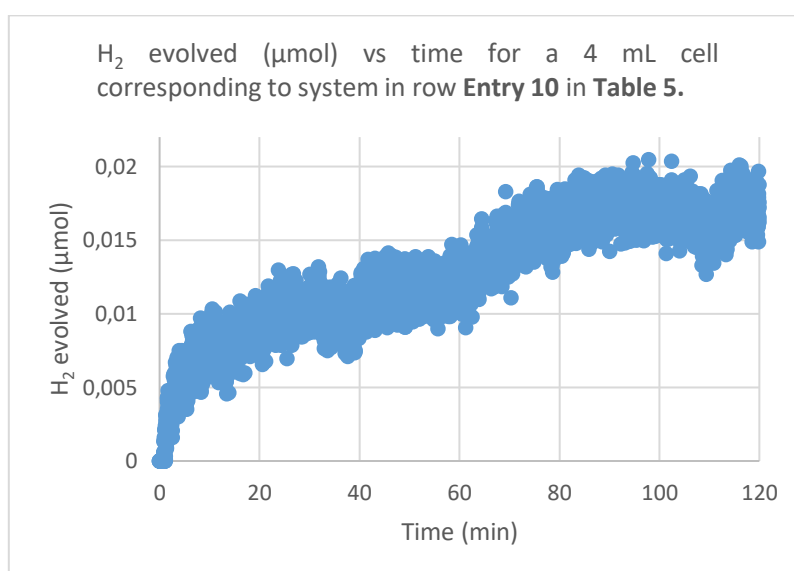


**Figure 12**. Plot of $H_2$ evolved (µmol) vs time for a 4 mL cell corresponding to the system in row **Entry 10** in **Table 5.**

The size of the Ru NPs should not be a determining factor for which our system fails to efficiently produce hydrogen since the tested Ru NPs were highly active when electrochemically triggered. ZnTCPP was tested to ensure that the system failure was not due to $[Ru(bpy)_3]^{2+}$. It was not the case, since both photosensitizers produced similar results.

Nevertheless, it turned out that the performance of the electron mediators was crucial to achieve results for photocatalytic proton reduction, as stated in reference [38]. Fukuzumi wrote about the importance of working with either a more efficient electron transfer electron mediator (in relation to methyl viologen) or a donor-acceptor linked photosensitizer when working with Ru NPs photocatalytically. The lack of neither the first nor the second might be the main cause of the inefficiency of our system.

Hydrogen gas was successfully produced but in low amounts. It is clear that the system needs improvement, needing to enhance the interaction between the components of the system. Thus, with this idea in mind it was decided to produce a hybrid material by mixing ruthenium nanoparticles with graphene oxide quantum dots to achieve the aforementioned Ru@GQDs@N-TiO$_2$ system, where TiO$_2$ is acting as the photoactive material (substitute of [Ru(bpy)$_3$]$^{2+}$) and GQDs are acting both as a stabilizing matrix for Ru NPs and as an electron reservoir for the hydrogen-evolving reaction.

### 4.4. Reduction of graphene quantum dots to form carbon micro-agglomerates

Here, it is reported for the first time the reduction of GQDs using NaBH$_4$ and CaCl$_2$. GQDs are highly oxidized materials possessing several polar groups on their surface that both decrease their conductivity (less aromaticity) and their dispersibility in organic solvents (less apolar). In order to increase both parameters it was decided to reduce them. Reasonable dispersibility in organic solvents is necessary to impregnate Ru NPs or decompose [Ru(cod)(cot)] as both chemical processes will be carried in THF, solvent in which both the Ru NPs and the [Ru(cod)(cot)] complex are dispersible. Increasing the conductivity means greater efficiency in the final photocatalytic system.
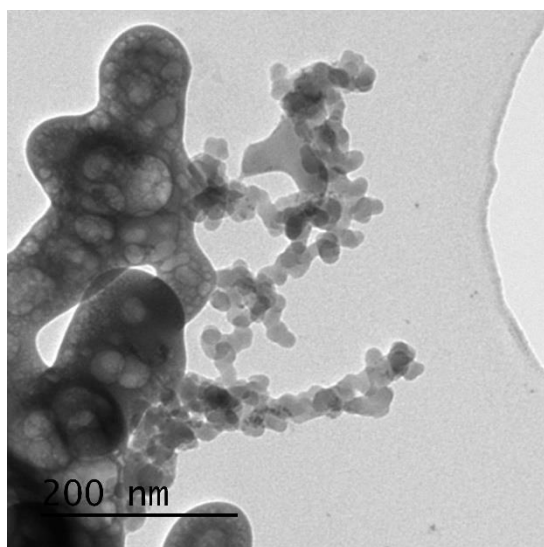


**Figure 13.** Reduced micro-agglomerate resultant from the reduction of GQDs.

Upon reduction GQDs are turned into porous-sponge-like micro-agglomerates (see **Figure 13**) with improved general dispersibility in organic solvents related to GQDs. Both GQDs and micro-agglomerates were tested in dry organic solvents and micro-agglomerates presented a superior dispersibility within them. Indeed, GQDs present a higher dispersibility in water than reduced micro-agglomerates. The reduced micro-agglomerates are grey-coloured materials with lower density than the parent black-coloured GQDs. EDX results reveal that the porous agglomerated material is composed of carbon and calcium. A hypothesis to explain the formation of this type of material is that reduction decreases the stability of GQDs as colloids in water and thus they become prone to aggregate either trapping calcium between agglomerated graphite layers or developing this element a structural function stabilizing the reduced material.

As a matter of fact and to clarify the terms: GQD is used for nanoparticles sized under 10 nm while agglomerates comprised between 10 and 100 nm are to be called nano-agglomerates and above 100 nm micro-agglomerates. Thus, our reduction of GQDs does not result in the formation of reduced graphene quantum dots but in reduced nano-/micro-agglomerates (see **Figure 13**).

## 4.5. Impregnation of Ru NPs onto graphene oxide quantum dots and reduced micro-agglomerates
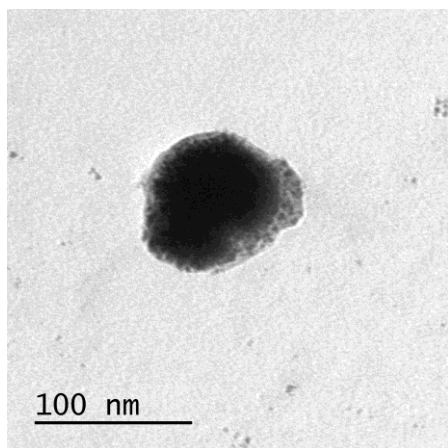


**Figure 14.** 100 nm agglomerates formed from the impregnation of Ru NPs (5%) onto GQDs.

To be impregnated, Ru-MPT (see **Table 2**) was chosen for two reasons: 1) it was thought that the smaller the NPs the better (Ru-MPT is sized between 1-2 nm) and 2) a large aromatic planar system like terpyridine was thought to be sensitive to interleaving ($\pi$ stacking) between the graphite layers of GQDs. Thus, having a larger matrix of GQDs or micro-agglomerate decorated with smaller Ru NPs. First impregnation was carried out with a 20% in weight of Ru NPs in respect to carbon material and it was decided that there was an excess of Ru, reason why a 5% was employed in all the following experiments.

The impregnation of Ru NPs onto GQDs resulted in the formation of agglomerates of about 100 nm (see **Figure 14**) in the precipitate fraction and carbon material in the supernatant. GQDs are highly polar and prefer being dispersed in water, while the impregnated material (containing poorly dispersible in water Ru NPs) tend to precipitate. The composition of the 100 nm agglomerates was assessed by EDX showing the presence of ruthenium in high concentrations. However, their carbon content could not be assessed by this technique due to the carbon content of the grids employed. Ru NPs do not agglomerate when placed in THF for long periods of time. Therefore, in principle this behaviour should be kept when placed together with GQDs in THF. Agglomeration is then explained by two possible hypothesis: 1) GQDs induce Ru NPs forming an agglomerate of the two and/or 2) GQDs induce Ru NPs agglomeration by removing 'somehow' the stabilizing ligands of the NPs. The latter would imply that stabilizing ligands are removed by GQDs.

GQDs and reduced micro-agglomerates were also placed overnight in THF to observe the contribution of THF to the agglomeration phenomena. The GQDs increased their size from 5-8 nm to 30 nm (see **Figure 15**), maybe due to their higher instability in THF than in water. With these results in hand, it can be hypothesised that there is an effect of aggregation due to both THF and Ru NPs when placed together with GQDs. In despite nothing happened to the reduced micro-agglomerates.
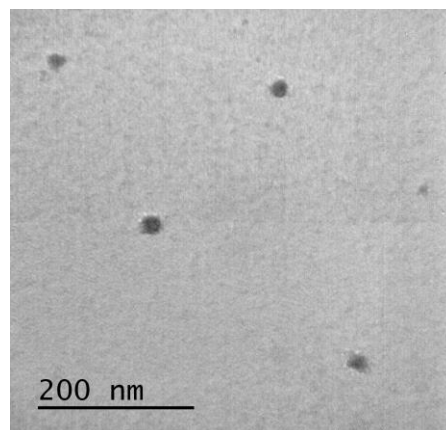


**Figure 15.** TEM image of GQDs left overnight in 1 mL THF.
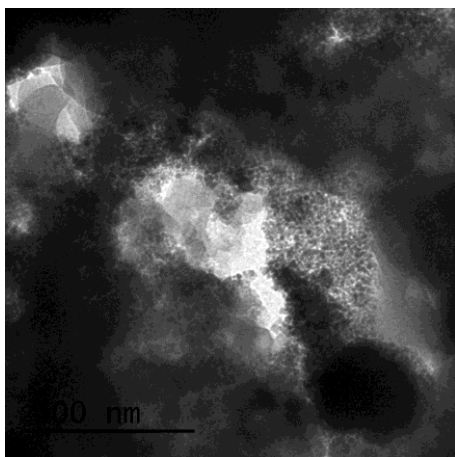
The impregnation on reduced micro-agglomerates seem to also lead to the formation of ruthenium-carbon agglomerates (see **Figure 16**).

**Figure 16.** TEM image of Ru NPs impregnated onto reduced migro-agglomerates.

### 4.6. Decomposition of [Ru(cod)(cot)] onto graphene oxide quantum dots and reduced micro-agglomerates

The decomposition of [Ru(cod)(cot)] onto GQDs lead to the formation of agglomerated carbon material due to the in situ one-pot reduction with hydrogen of organometallic complex and the dots with hydrogen, similar result to what happened when reducing the GQDs with sodium borohydride and calcium chloride. The material is found agglomerated with ruthenium on it (see **Figure 17**). The in situ reduction could indeed trap ruthenium inside the agglomerated material, a hypothetic explanation to the electrochemical results found within the following section.
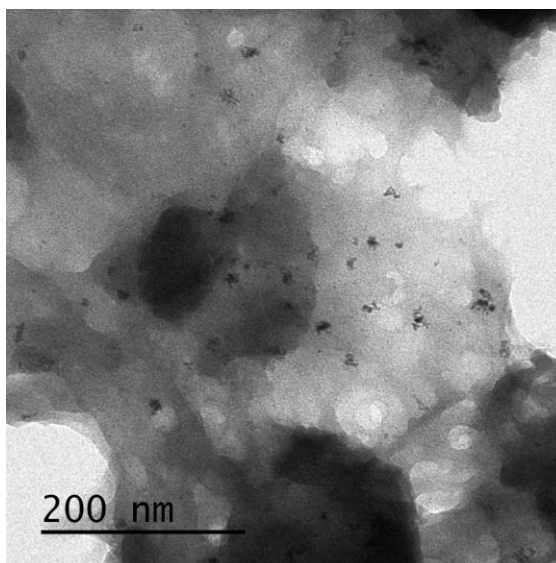


**Figure 17.** TEM image of [Ru(cod)(cot)] decomposed onto GQDs which leads to the formation of agglomerated carbon material.

The decomposition of [Ru(cod)(cot)] in the presence of the porous reduced micro-agglomerates leads to the formation of small Ru NPs all over the surface of the latter (see **Figure 18**). EDX results revealed that the porous agglomerated material is composed of carbon, calcium and ruthenium; see **Figure 26** in the **Supporting information.**
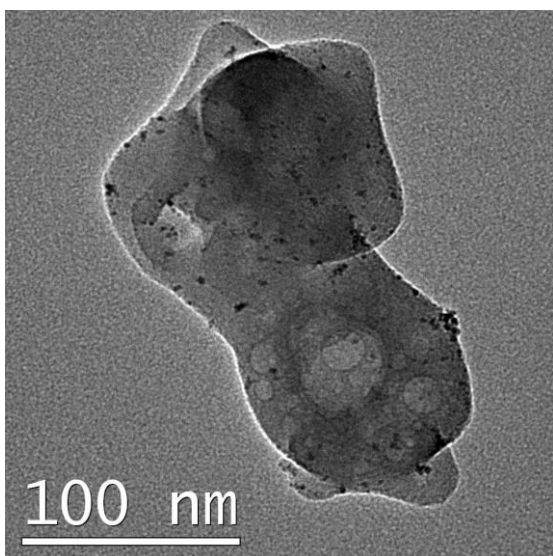


**Figure 18.** TEM image of [Ru(cod)(cot)] decomposed onto reduced porous micro-agglomerate.

## 4.7. Electrocatalytic evaluation of Ru@GQDs and Ru@reduced micro-agglomerates by impregnation and decomposition for hydrogen-evolving reaction

The Ru@GQDs and Ru@reduced micro-agglomerates both impregnated and decomposed were dispersed in THF (2 mg/mL) and sonicated in an ultrasound bath for 30 min. A 10 µL sample was added onto the surface of a glassy carbon rotating disk electrode (GC-RDE) (working electrode (WE), S = 0.07 cm$^2$) and allowed to dry under air. For electrochemical analysis, a 1 M $H_2SO_4$ solution was used, and a SCE and a Pt mesh were used as reference electrode and counter electrode, respectively.

Initially, a linear sweep voltammetry (LSV) was performed for each system, to test the primary activity. One representative LSV per sample is plotted in **Figure 19**:
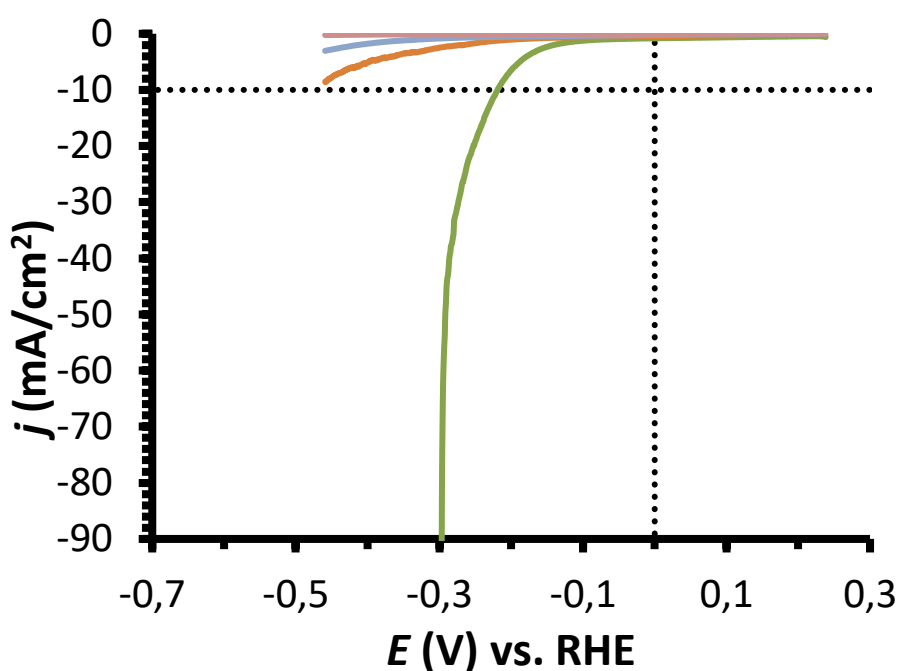


**Figure 19.** LSVs of a glassy carbon rotating disk electrode (GC-RDE) modified with: a) [Ru(cod)(cot)] decomposed onto reduced micro-agglomerate (green), b) [Ru(cod)(cot)] decomposed onto GQDs (orange), c) Ru-MPT impregnated onto reduced micro-agglomerate (blue) and d) Ru-MPT impregnated onto GQDs (pink). GC-RDE was used as working electrode, a saturated calomel electrode as reference and a Pt mesh as counter electrode. A 1 M $H_2SO_4$ (pH 0) solution was used as reaction media and proton source. The horizontal dotted line marks the value of overpotential at 10 mA/cm$^2$ while the vertical dotted line marks E=0.

**Figure 19** shows that the best performance corresponds to the system arising from the decomposition of [Ru(cod)(cot)] onto the reduced micro-agglomerate (green) with an onset overpotential (beginning of the catalytic wave) of 150 mV and an overpotential of 219 mV at a current density of 10 mA/cm$^2$, a typical electrocatalytic benchmarking value for hydrogen-evolving reaction. Compared to the available non-supported NPs (see **Table 2**), the supported system performs worse than Ru-MT (methanol and tetrahydrofurane stabilizing agents) and NPs containing pyridylic ligands as stabilizers (Ru-PP and Ru-MPT) but better than Ru-Ps, where a phosphine-type ligand stabilizes the system. However, it has to be remarked that the amount of metallic ruthenium is lower in the hybrid systems than in non-supported NPs. The rest of

systems ([Ru(cod)(cot)] decomposed onto GQDs (orange), Ru-MPT impregnated onto reduced micro-agglomerate (blue) and Ru-MPT impregnated onto GQDs (pink)) do not reach the 10 mA/cm$^2$ value at the studied potentials and do not present a clear onset overpotential. The onset overpotential (when catalysis starts) is characteristic for each catalyst and does not depend on its concentration while overpotential at 10 mA/cm$^2$ does depend on the concentration. In general, it could be said that the decomposed systems proportionate better results than the impregnated ones, maybe due to the high degree of agglomeration taking place during the impregnation of the formers (less catalytic area).

Then a chronopotentiometry (CP) was carried out, for an example see **Figure 20**. CP is a bulk electrolysis experiment, testing the evolution of the required overpotential to maintain a 10 mA/cm$^2$ current density within time. Less active systems (for instance [Ru(cod)(cot)] decomposed onto GQDs) provide clearer chronopotentiometries due to the absence of large hydrogen bubbles on the GC-RDE that could form during the process.
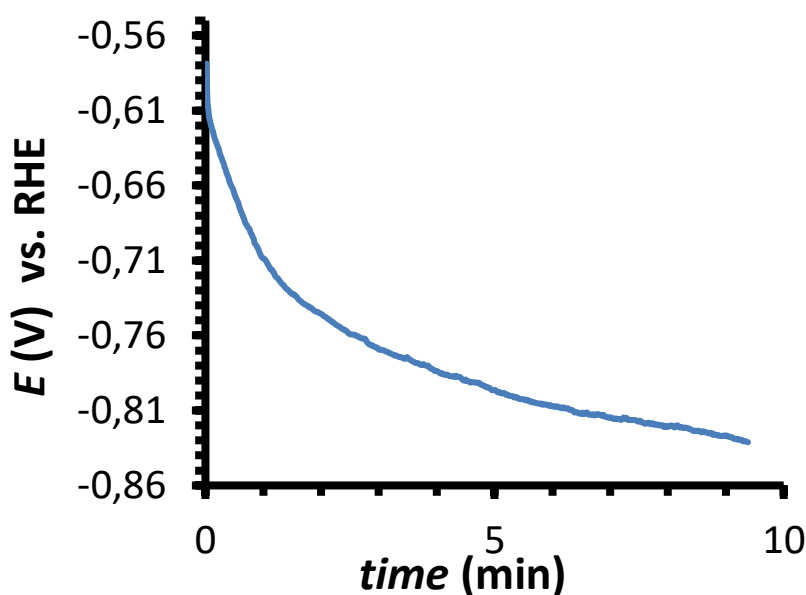


**Figure 20.** Chronopotentiometry experiment of a GC-RDE modified with [Ru(cod)(cot)] decomposed onto GQDs at j=10 mA/cm$^2$ (I=0.7 mA) for 10 min. Same conditions than the previous LSVs.

A stable material should maintain a constant overpotential along the experiment. If potential increases alongside time, it means that the material is non-stable and it is being deactivated. On the other hand if the potential decreases it means that the material is being activated. Normally, when performing CP experiments the potential tend to decrease due to the formation of huge H$_2$ bubbles on the active surface of the electrode, even when using a rotating disk electrode, impeding the proper electrochemical reduction of protons. For this reason, after the CP it is advised to carry out several LSVs and explain the tendencies with them in hand. Deactivated material will have higher overpotential at 10 mA/cm$^2$.

Finally, after the chronopotentiometry test, LSVs are performed to analyse the stability and robustness of the catalysts, see **Figure 21**.
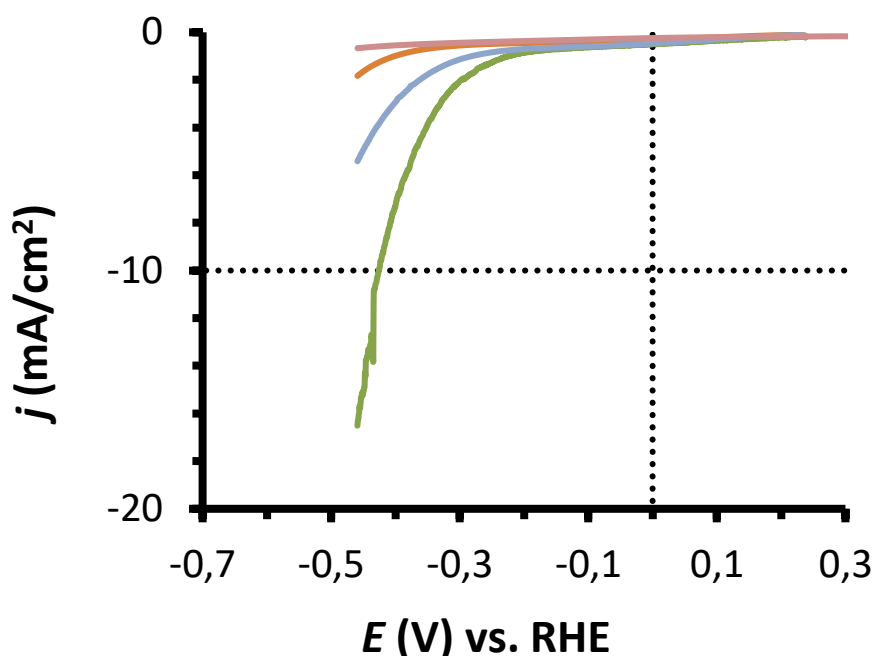
**Figure 21.** LSVs after the chronopotentiometry of a GC-RDE modified with: a) [Ru(cod)(cot)] decomposed onto reduced micro-agglomerate (green), b) [Ru(cod)(cot)] decomposed onto GQDs (orange), c) Ru-MPT impregnated onto reduced micro-agglomerate (blue) and d) Ru-MPT impregnated onto GQDs (pink). Same conditions than the previous LSVs.

In general, the activity of impregnated Ru-MPT onto carbon material (blue and pink) has increased. This is due to the activation of the Ru NPs by removing a passivation surface oxide layer. This same trend was detected by PhD students from SelOxCat when assessing the electrocatalytic properties of the Ru NPs alone.

The activity has experienced a considerable decrease for [Ru(cod)(cot)] decomposed onto carbon material (green and orange). Still green being the most active but with an onset overpotential of 300 mV and an overpotential at 10 mA/cm$^2$ of 426 mV. The decrease of activity of this system (green) is attributed to a loss of the active material falling from the electrode more than to the deactivation of the catalyst itself. This hypothesis comes from the fact that when finishing a concrete electrochemical experiment using the reduced micro-agglomerate matrix (both for decomposition and impregnation), the material was found in smaller amounts on the electrode when cleaning and washing it. Future electrochemical experiments should focus on increasing the adherence of the [Ru(cod)(cot)] decomposed onto reduced micro-agglomerate onto the electrode by using Nafion, a stabilizing polymer which acts as glue between the electrode and the catalytic material, or by replacing the glassy carbon rotating disk electrode by a fluorine doped tin oxide (FTO) electrode.

## 5. Conclusions

In conclusion, in this work hydrogen gas has been photocatalytically produced with Ru NPs but in low amounts. It is clear that the systems need improvement, needing to enhance the interaction between the different components (Ru NPs, PS, EM and SED). Thus, with this idea in mind it was decided to produce a hybrid material by mixing ruthenium nanoparticles with graphene oxide quantum dots or reduced micro-agglomerates. The latter previously synthesised from the reduction of GQDs. Reduced micro-agglomerates or GQDs should act as a linking-conductive-matrix improving the interaction with N-TiO$_2$. The best results were given by the [Ru(cod)(cot)] decomposed on reduced micro-agglomerates, although catalytic material was removed from the electrode over time. These materials are of high interest, exhibiting unique properties, but also are poorly understood and highly complex to work with.

In the future it should be mandatory to check electrochemistry with Nafion (stabilizing polymer acting as glue between the electrode and the catalytic material) or FTO that can stabilize more efficiently the catalytic material on its surface to avoid material loss. This would allow checking properly the stability and robustness of the catalyst by using chronopotentiometry.

The lack of time has impeded us to fully develop and characterise the cake-like system Ru@GQDs@N-TiO$_2$ composed of a larger photoactive TiO$_2$ matrix with Ru@GQDs embedded onto its surface. Ultimately, it should be fully developed and photocatalytically tested in the future.

## 6. References

[1]     S. Shafiee and E. Topal, "When will fossil fuel reserves be diminished?," *Energy Policy*, vol. 37, pp. 181–189, 2009.

[2]     M. I. Hoffert, "Farewell to Fossil Fuels ?," *Clim. Chang.*, vol. 329, no. September, pp. 1292–1295, 2010.

[3]     M. I. Hoffert, K. Caldeira, A. K. Jain, E. F. Haites, L. D. D. Harveyk, S. D. Potter, S. H. S. Michael E. Schlesinger, R. G.Watts, T. M. L. Wigley, and D. J.Wuebbles, "Energy implications of future stabilization of atmospheric CO2 content," *Nature*, vol. 395, no. October, pp. 881–884, 1998.

[4]     F. Birol and D. Millard, "Key world energy statistics," *Int. Energy Agency*, pp. 1–80, 2016.

[5]     L. Baratas, "Consumo y derroche de energía en el planeta: ¿podemos resistir?," *Econonuestra*, 2014. [Online]. Available: http://econonuestra.org/actualidad/item/924-consumo-y-derroche-de-energ%25C3%25ADa-en-el-planeta-%25C2%25BFpodemos-resistir?.html. [Accessed: 08-Apr-2017].

[6]     G. Rothenberg, *Catalysis - Concepts and Green Applications*. Weinheim: WILEY-VCH Verlag GmbH & Co. KGaA, 2008.

[7]     J. C. Rogers, E. A. Simmons, I. Convery, and A. Weatherall, "Social impacts of community renewable energy projects : findings from a woodfuel case study," *Energy Policy*, vol. 42, pp. 239–247, 2012.

[8]     P. Devine-Wright, "Reconsidering public attitudes and public acceptance of renewable energy technologies : a critical review," *Econ. Soc. Res. Counc.*, no. February, pp. 1–15, 2007.

[9]     W. Schreiber, "Solving the Energy Problem," *MIT Faculty Newsletter*, 2007. [Online]. Available: http://web.mit.edu/fnl/volume/196/schreiber.html. [Accessed: 08-Apr-2017].

[10]    "Available energy." [Online]. Available: https://upload.wikimedia.org/wikipedia/commons/thumb/8/81/Available_Energy-3-es.png/250px-Available_Energy-3-es.png. [Accessed: 08-May-2017].

[11]    M. A. Green, K. Emery, Y. H. W. Warta, and E. D. Dunlop, "Solar cell efficiency tables (version 47)," *Prog. Photovoltaics*, vol. 24, pp. 3–11, 2016.

[12]    H. YAN and G. ZHANG, "Prof. Yan's Research Group, Frontier Research Group in Organic Photovoltaics." [Online]. Available: blog.ust.hk/yanlab/. [Accessed: 10-Apr-2017].

[13]    K. M. Macounová, N. Simic, E. Ahlberg, and P. Krtil, "Electrochemical Water-Splitting Based on Hypochlorite Oxidation," *J. Am. Chem. Soc.*, vol. 137, p. 7262–7265, 2015.

[14]    G. F. Naterer, I. Dincer, and C. Zamfirescu, *Hydrogen Production from Nuclear Energy*. London: Springer-Verlag, 2013.

[15]    J. E. Funk, "Thermochemical hydrogen production: past and present," *Int. J. Hydrogen Energy*, vol. 26, pp. 185–190, 2001.

[16]    A. Eftekhari, V. J. Babu, and S. Ramakrishna, "Photoelectrode nanomaterials for photoelectrochemical water splitting," *Int. J. Hydrogen Energy*, vol. 30, pp. 1–32, 2017.

[17]    T. Melis, R. Garland, and L. Yancey, "II . F . 2 Maximizing Light Utilization Efficiency and Hydrogen Production in Microalgal Cultures," University of California, Berkeley, 2008.

[18]    R. M. N. Yerga, M. C. Galván Álvarez, F. Valle Del, J. Villoria de la Mano, and J. L. G. Fierro, "Water Splitting on Semiconductor Catalysts under Visible- Light Irradiation," *ChemSusChem*, vol. 2, pp. 471–485, 2009.

[19]    S. Dunn, *Encyclopedia of Energy*. Amsterdam: Elsevier, 2004.

[20]    M. Momirlan and T. N. Veziroglu, "The properties of hydrogen as fuel tomorrow in sustainable energy system for a cleaner planet," *Int. J. Hydrogen Energy*, vol. 30, pp. 795–802, 2005.

[21]    Y. Yamada, T. Miyahigashi, H. Kotani, K. Ohkubo, and S. Fukuzumi, "Photocatalytic Hydrogen Evolution

under Highly Basic Conditions by Using Ru Nanoparticles and 2-Phenyl-4- ( 1-naphthyl ) quinolinium Ion," *J. Am. Chem. Soc.*, vol. 133, pp. 16136–16145, 2011.

[22]     J. Mahmood, F. Li, S. Jung, M. S. Okkay, I. Ahmad, S. Kim, N. Park, H. Y. Jeong, and J. Baek, "An ef fi cient and pH-universal ruthenium-based catalyst for the hydrogen evolution reaction," *Nat. Nanotechnol.*, no. February, pp. 1–7, 2017.

[23]     J. Lu, J. Yang, J. Wang, A. Lim, S. Wang, and K. P. Loh, "One-Pot Synthesis of Fluorescent Carbon Graphene by the Exfoliation of Graphite in Ionic Liquids," *ACS Nano*, vol. 3, no. 8, pp. 2367–2375, 2009.

[24]     H. Ming, Z. Ma, Y. Liu, K. Pan, H. Yu, F. Wang, and Z. Kang, "Large scale electrochemical synthesis of high quality carbon nanodots and their photocatalytic property," *Dalt. Trans.*, vol. 41, pp. 1–5, 2012.

[25]     Y. Yuan, H. Lu, Z. Ji, J. Zhong, M. Ding, D. Chen, Y. Li, W. Tu, D. Cao, Z. Yu, and Z. Zou, "Enhanced visible-light-induced hydrogen evolution from water in a noble-metal-free system catalyzed by ZnTCPP-MoS2/TiO2 assembly," *Chem. Eng. J.*, vol. 275, pp. 8–16, 2015.

[26]     H. Yu, H. Zhang, H. Huang, Y. Liu, H. Li, and H. Ming, "ZnO/carbon quantum dots nanocomposites: one-step fabrication and superior photocatalytic ability for toxic gas degradation under visible light at room temperature," *New J. Chem.*, vol. 36, pp. 1031–1035, 2012.

[27]     Y. Kobayashia, T. Iwasakia, K. Kageyamab, S. Ishikurob, K. Yamasakic, T. Yonezawac, and A. Takenoshita, "Colloids and Surfaces A : Physicochemical and Engineering Aspects Fabrication of nitrogen-doped titanium oxide/silica core–shell particles and their electrical conductivity," *Colloids Surfaces A Physicochem. Eng. Asp.*, vol. 457, pp. 244–249, 2014.

[28]     "A recipe calculator for thermodynamically correct buffers for pH control - Centre for Proteome Research, Liverpool." [Online]. Available: https://www.liverpool.ac.uk/buffers/buffercalc.html. [Accessed: 02-Jun-2017].

[29]     M. R. Norris, J. J. Concepcion, C. R. K. Glasson, Z. Fang, A. M. Lapides, D. L. Ashford, J. L. Templeton, and T. J. Meyer, "Synthesis of Phosphonic Acid Derivatized Bipyridine Ligands and Their Ruthenium Complexes," *Inorg. Chem.*, vol. 52, pp. 12492–12501, 2013.

[30]     G. Villemure and T. J. Pinnavaia, "Cyclic Voltammetry of Tris (2,2'-bipyridyl) ruthenium (II) Cations Adsorbed in Electrodes Modified with Mesoporous Molecular Sieve Silicas," *Chem. Mater.*, vol. 11, pp. 789–794, 1999.

[31]     M. Matsui, M. Miyano, and K. Tomita, "Calcium Borohydride Reduction of Ketoesters," *Bull. Agr. Chem. Soc. Japan*, vol. 20, no. 3, pp. 139–140, 1956.

[32]     C. A. Practical, "Stereoselective Reduction of Epoxy Ketones with Sodium Borohydride in the Presence of Calcium Chloride or Lanthanum Chloride. A Practical Preparation of erythro-Epoxy Alcohols," *Tetrahedron*, vol. 51, no. 3, pp. 679–686, 1995.

[33]     M. Periasamy and M. Thirumalaikumar, "Methods of enhancement of reactivity and selectivity of sodium borohydride for applications in organic synthesis," *J. Organomet. Chem.*, vol. 609, pp. 137–151, 2000.

[34]     Z. Yang, Q. Zheng, H. Qiu, J. Li, and J. Yang, "A simple method for the reduction of graphene oxide by sodium borohydride with CaCl2 as a catalyst," *New Carbon Mater.*, vol. 30, no. 1, pp. 41–47, 2015.

[35]     S. Fukuzumi and Y. Yamada, "Catalytic activity of metal-based nanoparticles for photocatalytic water oxidation and reduction," *J. Mater. Chem.*, vol. 22, pp. 24284–24296, 2012.

[36]     C. C. L. McCrory, S. Jung, J. C. Peters, and T. F. Jaramillo, "Benchmarking Heterogeneous Electrocatalysts for the Oxygen Evolution Reaction," *J. Am. Chem. Soc.*, vol. 135, p. 16977–16987, 2013.

[37]     Y. Yamada, T. Miyahigashi, H. Kotani, K. Ohkuboa, and S. Fukuzumi, "Photocatalytic hydrogen evolution with Ni nanoparticles by using 2-phenyl-4-(1-naphthyl)quinolinium ion as a photocatalyst," *Energy Environ. Sci.*, vol. 5, pp. 6111–6118, 2012.

[38]    Y. Yamada, A. K. Yano, and S. F. A, "Photocatalytic Hydrogen Evolution Using 9-Phenyl-10- methyl-acridinium Ion Derivatives as Efficient Electron Mediators and Ru-Based Catalysts," *Aust. J. Chem.*, no. 65, pp. 1573–1581, 2012.

[39]    Y. Yamada, T. Miyahigashi, K. Ohkuboa, and S. Fukuzumi, "Photocatalytic hydrogen evolution from carbon-neutral oxalate with 2-phenyl-4-(1-naphthyl)quinolinium ion and metal nanoparticles," *Phys. Chem. Chem. Phys.*, vol. 14, pp. 10564–10571, 2012.

[40]    S. Fukuzumi and K. Ohkubo, "Photoinduced Reactions of Radical Ions via Charge Separation," *Encycl. Radicals Chem. Biol. Mater.*, vol. 1, pp. 1–29, 2012.

[41]    Y. Yamada, S. Shikano, and S. Fukuzumi, "Robustness of Ru/SiO 2 as a Hydrogen-Evolution Catalyst in a Photocatalytic System Using an Organic Photocatalyst," *J. Phys. Chem.*, vol. 117, pp. 13143–13152, 2013.

[42]    Y. Pellegrin and F. Odobel, "Sacrificial electron donor reagents for solar fuel production," *Comptes Rendus Chim.*, vol. XXX, pp. 1–13, 2016.

[43]    C. Creutz, N. Sutin, and B. S. Brunschwig, "Homogeneous Catalysis of the Photoreduction of Water by Visible Light. Mediation by a Tris(2,2'-bipyridine)ruthenium(II)-Cobalt(II) Macrocycle System," *J. Am. Chem. Soc.*, vol. 101, no. 5, pp. 1298–1300, 1979.

[44]    C. V. Krishnan and N. Sutin, "Homogeneous Catalysis of the Photoreduction of Water by Visible Light. 2. Mediation by a Tris( 2,2'-bipyridine)ruthenium( 11)-Cobalt(I1) Bipyridine System," *J. Am. Chem. Soc.*, vol. 103, pp. 2141–2142, 1981.

[45]    M. Meilikhov, K. Yusenko, D. Esken, S. Turner, G. Van Tendeloo, and R. A. Fischer, "Metals @ MOFs – Loading MOFs with Metal Nanoparticles for Hybrid Functions," *Eur. J. Inorg. Chem.*, vol. 1, pp. 3701–3714, 2010.

[46]    W. Fan, Q. Zhang, and Y. Wang, "Semiconductor-based nanocomposites for photocatalytic H2 production and CO2 conversion," *Phys. Chem.*, vol. 15, pp. 2632–2649, 2013.

[47]    J. Liu, L. L. Zhang, J. Zhang, T. Liu, and X. S. Zhao, "Bimetallic ruthenium – copper nanoparticles embedded in mesoporous carbon as an ff ective hydrogenation catalyst †," *Nanoscale*, vol. 5, pp. 11044–11050, 2013.

[48]    H. Bi, X. Tan, R. Dou, Y. Pei, M. Qiao, B. Sun, and B. Zong, "Ru–B nanoparticles on metal-organic frameworks as excellent catalysts for hydrogenation of benzene to cyclohexane under mild reaction conditions," *Green Chem.*, vol. 18, pp. 2216–2221, 2016.

[49]    F. Schröder, D. Esken, M. Cokoja, M. W. E. Van Den Berg, O. I. Lebedev, G. Van Tendeloo, B. Walaszek, G. Buntkowsky, H. Limbach, B. Chaudret, and R. A. Fischer, "Ruthenium Nanoparticles inside Porous [Zn4O(bdc)3] by Hydrogenolysis of Adsorbed [Ru(cod)(cot)]: A Solid-State Reference System for Surfactant-Stabilized Ruthenium Colloids," *J. Am. Chem. Soc.*, vol. 130, pp. 6119–6130, 2008.

[50]    Y. Zhao, J. Zhang, J. Song, J. Li, J. Liu, T. Wu, and P. Zhang, "Green Chemistry Ru nanoparticles immobilized on metal – organic framework nanorods by supercritical CO 2 -methanol solution : highly efficient catalyst," *Green Chem.*, vol. 13, pp. 2078–2082, 2011.

[51]    A. Dhakshinamoorthy and H. Garcia, "Chem Soc Rev Catalysis by metal nanoparticles embedded on metal – organic frameworks," *Chem. Soc. Rev.*, vol. 41, pp. 5262–5284, 2012.

[52]    H. Bi, X. Tan, R. Dou, Y. Pei, and M. Qiao, "Ru – B nanoparticles on metal-organic framework as excellent catalyst for benzene hydrogenation to cyclohexane under mild reaction conditions," *Green Chem.*, vol. 53, pp. 1–9, 2015.

[53]    T. Zhang, Z. Wang, Q. Zhao, F. Li, and W. Xue, "Partial Hydrogenation of Benzene to Cyclohexene over Ru-Zn / MCM-41," *J. Nanomater.*, vol. 1, pp. 1–8, 2015.

[54]    Y. Yang, C. Sun, D. E. Brown, L. Zhang, and F. Yang, "A smart strategy to fabricate Ru nanoparticle inserted porous carbon nano fi bers as highly e ffi cient levulinic acid hydrogenation catalysts," *Green Chem.*, vol. 18, pp. 3558–3566, 2016.

## 7. Supporting information
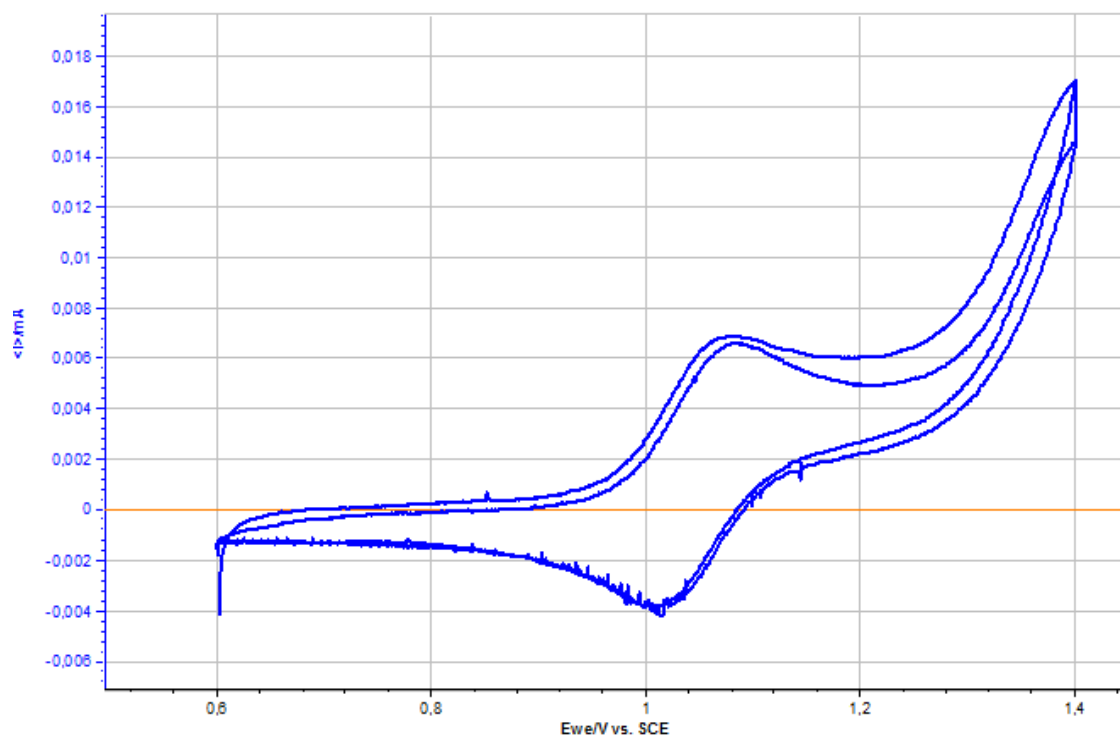
### 7.1. Cyclic voltammetries



**Figure 22.** Registered cyclic voltammetry for the synthesised $[Ru(bpy)_3]^{2+}$.



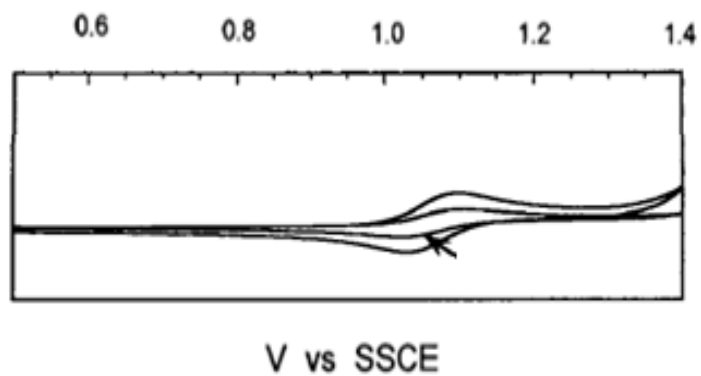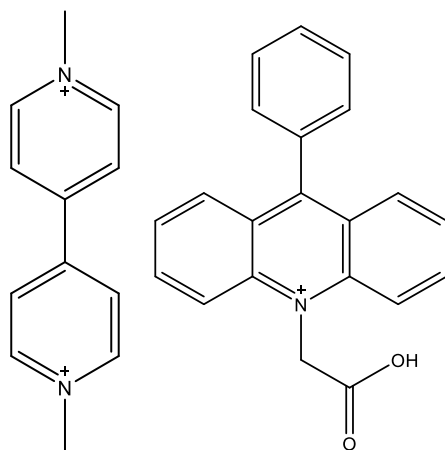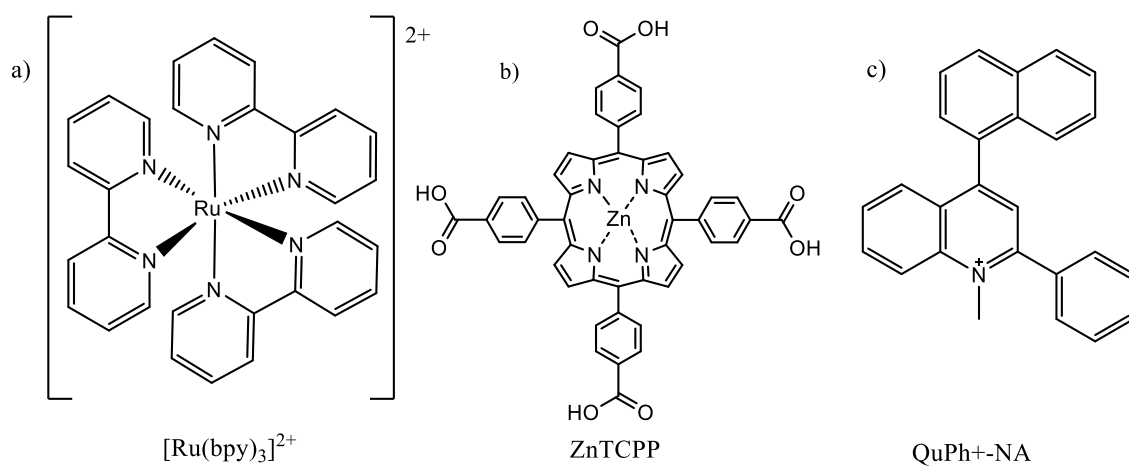**Figure 23.** Literature $[Ru(bpy)_3]^{2+}$ cyclic voltammetry [30].

## 7.2. Chemical structures of related compounds

**Figure 24.** On the left, methyl viologen chemical structure. On the right, PMAID chemical structure.

a)                                   b)                                   c)

[Ru(bpy)₃]²⁺                          ZnTCPP                               QuPh+-NA

$[Ru(bpy)_3]^{2+}$      ZnTCPP      QuPh+-NA

**Figure 25.** Structures of the PSs mentioned in the report.

## 7.3. EDX of [Ru(cod)(cot)] decomposed onto reduced micro-agglomerate



**Figure 26.** EDX results revealed that the porous agglomerated material is composed of carbon, calcium and ruthenium after the decomposition of [Ru(cod)(cot)].

**7.4. Safety Data Sheets (SDSs)**

Safety data sheets of most dangerous reagents and solvents used in the report: methyl viologen, sodium borohydride, sodium perchlorate, tetrahydrofuran and toluene.

Not exempt from danger, but less dangerous (SDS not included): 2,2'-bipyridyl, calcium chloride, ethanol, phosphoric acid, potassium oxalate, ruthenium(III) chloride hydrate, sodium hydrogen sulphate, sodium phosphate and sulphuric acid among others.

Non-hazardous (SDS not included): ascorbic acid, sodium sulphate and triethanolamine.